Promising Antioxidant, Antibacterial and Anticorrosive Properties of an Essential Oil Extract of *Origanum Majorana L.* from Morocco

Malika Sabiha [1] iD, **Siham Yanisse** [2], **Maria Boudalia** [1], **Ayoub Najem** [1,3], **Fouad Benhiba** [4], **Amin Belfhaili** [1], **Siham Echihi** [1,5], **Nabila Chahboun** [1,6,7], **Abdallah Guenbour** [1], **Ismail Warad** [8], **Abdelkabir Bellaouchou** [1], **Abdelkader Zarrouk** [1,*] iD, **Mustapha Bouatia** [2]

[1] Laboratory of Materials, Nanotechnology and Environment, Faculty of Sciences, Mohammed V University in Rabat, Av. Ibn Battouta, P. O. Box 1014 Agdal-Rabat, Morocco
[2] Team of Formulation and Quality Control of Health Products, Faculty of Medicine and Pharmacy, Mohammed V University in Rabat, Morocco
[3] Institute of Pharmacognosy, Interdisciplinary Excellence Centre, University of Szeged, Szeged, Hungary
[4] Laboratory of Advanced Materials and Process Engineering, Faculty of Sciences, Ibn Tofail University, B.P 242, 14000 Kenitra, Morocco
[5] Laboratory of Materials Engineering for the Environment and Natural Resources, Faculty of Sciences and Techniques, University Moulay Ismail of Meknes BP 509 Boutalamine 52000 Errachidia, Morocco
[6] Laboratory of Natural Resources and Sustainable Development, Faculty of Sciences, Ibn Tofail University, P.O. Box 242, 14000, Kenitra, Morocco
[7] Institute of Nursing Professions and Health Techniques, Annex Taza, Morocco
[8] Department of Chemistry, AN-Najah National University, P.O. Box 7, Nablus, Palestine
* Correspondence: azarrouk@gmail.com (A.Z.);

Abstract: Origanum Majorana L. from Errachidia region (Morocco) was the matrix subjected during this work. The essential oil was obtained by hydrodistillation using the Clevenger system. Chemical composition was recognized using the chromatographic method (GC-MS). The yield of Origanum Majorana L. essential oil (OML-EO) was considerable (1.92%), and the chemical composition showed that terpene-4-ol is the major compound with an important percentage of 39.59 %. Antioxidant activity was determined using three different tests: DPPH, ABTS, and FRAP assays. The IC50 in the DPPH assay has an interesting antioxidant activity surrounding 4.006 mg/mL. ABTS and FRAP tests were in agreement with the DPPH test. The antibacterial activity was determined using the microdilution method, and it shows an effective against strains *Staphylococcus aureus*, *Escherichia coli*, *Bacillus subtilis,* and *Pseudomonas aeruginosa*. The anticorrosion activity was conducted via ferrous steel in an acidic environment. This research was adopted via polarization curves and Electrochemical impedance spectroscopic (EIS) plots, indicating that *OML-EO* exhibited protective properties and reacted as a suitable corrosion inhibitor in an acidic environment. The protective capacity was as high as 94% for 0.5 g/L of this essential oil, which manifested itself as a barrier layer by Scanning Electron Microscopy (SEM). The computational chemistry (DFT) method and Molecular Dynamics (MD) simulation were utilized to rationalize the inhibitory effect and adsorption mode. Therefore, the tested plant has various applications with good results, opening interesting perspectives of other applications for these OML-EO.

Keywords: *Origanum Majorana.L*; GC-MS; antioxidant; antibacterial; anticorrosion; DFT/MD.

1. Introduction

Natural resources, in particular plants, were used for decades. The main usefulness was curing disease. Traditional healers are knowledgeable persons, giving prescriptions transferred from generation to generation. Encouraging human beings to use them is not hazardous due to their interesting properties and pharmacological benefits. The pivot role of plants against several diseases comes from the valuable volatiles' compounds, and no volatile compounds constituents are present in the substrate. Varieties of bioactive compounds deal with specific targets against several damages. Essential oils are considered as prize material recovered from plants. Their ability to neutralize free radicals causing cell damage was evaluated in many scientific productions [1]. They might be used as antibacterial agents [2,3], antifungal elements, and antiproliferative [4,5]. Orientation to natural products takes the attention of many classes of people around the world. Due to the safety provided and no need to be bothered.

On the other hand, synthetic products possess secondary effects, and they cause damage in the long term [6,7]; sometimes, they produce viral diseases [8]. Oxidative stress is considered a leading agent in several chronic diseases [1]. Numerous persons suffer from oxidative stress. He destroys and worsens cells and damages the organism's function. Looking forward to discovering antioxidant agents is a contributing path. Many authors reported using the essential oil and botanical extracts as antioxidant elements to reduce oxidative stress [9]. Enhancing the bioavailability of reductors is so beneficial, particularly from natural resources (plants, herbs, fruits). The origanum plant is known to contain tremendous amounts of antioxidants [10–12]. Essential oil and plant components such as Polyphenols and flavonoids have been studied as natural antioxidants which can serve the human body in reducing oxidative damage caused by free radicals [13]. Those antioxidants mainly neutralize free radicals, such as reactive oxygen species (ROS).

Most mitigating corrosion products contain various functional groups, such as C-O, C-H, C=O, O-H, and CHO [14-18]. The above-mentioned compounds are adsorbed and form a protective layer on the steel's surface to limit corrosion formation [19-21]. Green anticorrosion inhibitors recently occupied a predominant place in the industry as an alternative to synthetic compounds [22]. Essential oils extracted from natural plants are highly obtainable products with corrosion-preventing properties and renewable sources; by nature, they are non-toxic [23,24]. Many chemical components are present in these plant essential oils, such as terpene, polyphenols, and aromatic rings. These compounds have the ability to slow down the corrosion process of steel [14,25–28]. Hydrochloric acid is considered a commonly examined medium due to its wide use in the industry [29]. Indeed, steel is the most frequency used due to its adequate cost [30]. Several studies were conducted in this medium using theoretical and experimental approaches to give more insights into corrosion efficiency [31-33].

This leads us to reflect on anticorrosion tests using both approaches mentioned to check the limit of protection against the degradation of the Ferrous metal involved.

We aim to study the *Origanum Majorana L.*, Vernacular named "Merdedûch" [34]. This plant is one of the species *origanum* of the labiate family. We selected this plant precisely because it is widely abundant in Morocco, as well as there is no reported study combining the three intended activities. Moreover, there is no detailed examination regarding the use of this plant from the Errachidia region in corrosion inhibition [32,33]. The Chemical profiling of the essential oil was assayed by using gas chromatography coupled with mass spectroscopy (GC-MS), and the evaluation of both antioxidant and antimicrobial activities will be conducted using

DPPH, ABTS, FRAP, and MIC. Electrochemical techniques (PDP, EIS), scanning electron microscope (SEM), X-Ray diffraction, UV-liquid, and DFT tools will be assessed regarding the anticorrosion part.

2. Materials and Methods

2.1. Plant material.

The substrate used in this experiment for antioxidant activity was collected from wild-growing arias of Morocco (Errachidia provinces) in seasons (2020). It was freshly harvested, washed, and air-dried for fifteen days at room temperature. This species was identified at the Department of Botany and Plant Ecology, Institute Scientific University of Rabat, and registered under voucher number (RAB111870). The specimen was deposited in the plant section of the herbarium at the Institute Scientific University of Rabat.

2.1.1. Preparation of essential oil.

200 g of aerial parts from *O. Majorana* L. were hydrodistilled for 4 hours using a Clevenger-style apparatus, filtered to remove any remaining water, and then kept at +4°C in the dark until being tested and evaluated. To calculate the EOs' yields, the extraction was carried out many times.

2.1.2. Chemical analysis of volatile constituents.

A gas chromatograph (Perkin Elmer ClarusTM GC-680) and a mass spectrometer were used for the analysis (Q-8 MS). Samples of essential oils (0.5 µL) were directly injected into the HP-5MS column, which has a length of 60 m, an internal diameter of 0.25 mm, and a film thickness of 0.25 mm. the following analytical conditions: With a flow rate of 1 µL min^{-1}, a temperature range of 60°C to 300°C at a rate of 2°C/min, and injector and interface temperatures of 280°C and 300°C, respectively, were set, helium was employed as the carrier gas. A quadrupole mass spectrometer that ran at 70 V was used to conduct the GC/mass spectrometry (MS) study. The area of the chromatographic peaks was used to compute the percentage compositions of the essential oils. The sample was solubilized in hexane (1 ppm). Peak identification was based on the mass spectra of each compound with the use of the NIST database.

2.2. Study of the antioxidant activity.

2.2.1. Scavenging effect on 1,1-diphenyl-2-picrylhydrazyl (DPPH assay).

The DPPH test was carried out as described by Hatano *et al*.[35], with some modifications. Briefly, 1 mL aliquot of various essential oil dilutions and its main active compounds were mixed with 0.5 mL of a 99.98% methanol solution of DPPH (0.02 mM). After an incubation period of 30 min at room temperature, the absorbance of the samples was read at wavelength 517 nm using a spectrophotometer. Ascorbic acid is used as positive control. Percentage inhibition (PI %) of free radical DPPH was calculated as follows the equation (1):

$$PI(\%) = \left[\frac{A(blank) - A(sample)}{A(blank)}\right] \times 100 \tag{1}$$

$A(blank)$ is the absorbance of the control reaction and $A(sample)$ is the absorbance in the existence of the tested extract.

2.2.2. ABTS radical scavenging assay.

The analysis was made following the protocol described by Re *et al.* [36]. A stock solution of 7 mM ABTS was added to an equal volume of 2.45 mM potassium persulphate stock sample solution, and the obtained mixture was stored for 24h at 25°C in the dark. Methanol was added to reach 0.7±0.2 units very carefully at wavelength 734 nm. Then, 2 mL of the obtained solution was added to 200 µL of the crude extract, the whole was mixed, and the absorbance was registered at wavelength 734 nm. The results were determined using the following equation (2): ABTS radical scavenging activity:

$$\% \, Inhibition = \left[\frac{Abs(blank) - Abs(sample)}{Abs(blank)} \right] \times 100 \tag{2}$$

where $Abs(blank)$ represents the read value of the blank and $Abs(sample)$ is the read value of the test sample.

2.2.3. FRAP assay.

The reducing power was examined following the protocol of Oyaizu [37]. Each extract in methanol and water (2.5 mL) was mixed with 2.5 mL of 200 mM of sodium phosphate buffer, and 2.5 mL of 1% potassium ferricyanide, and the mixture was incubated at 50°C for 20 min. Then, 2.5 mL of 10% trichloroacetic acid was added, and the resulting solution was centrifuged for 10 min. The upper layer (2.5 mL) was mixed with 2.5 mL deionized water and 0.5 mL of ferric chloride (FeCl3 0.1 %). Then, the absorbance was noticed at wavelength 700 nm.

2.3. Antimicrobial activity.

2.3.1. Microorganisms and cultivated conditions.

The choice of bacteria was based on the strains of bacteria frequent in human pathology, belonging to two categories (*Gram Positive* and *Gram Negative*). These bacterial species are often responsible for nosocomial infections, which constitute a major public health problem. The following microorganisms were examined to see whether *OML*-essential oil has any antibacterial properties: The laboratory of the Team of Formulation and Quality Control of Health Products, Faculty of Medicine and Pharmacy, Mohammed V University in Rabat provided the *Gram Positive* (*Staphylococcus aureus* and *Bacillus subtilis*) and *Gram Negative* (*Escherichia coli* and *Pseudomonas aeruginosa*) bacteria. The pathogens' bacterial strains were cultivated on YPGA medium (5 g yeast extract, 5 g peptone, 10 g glucose, 15-18 g agar, in 1 liter) and incubated at 28°C before being grown at 37°C in Mueller-Hinton agar (MHA). The experiment employed final inoculum doses of 106 CFU/mL.

2.3.2. Minimum Inhibitory Concentration (MIC).

The plant's definition of the Minimum Inhibitory Concentration (MIC) is the lowest inhibitor concentration at which the microorganism does not exhibit discernible growth

following incubation. 20 L of Risazurin (1 mg/mL) diluted in sterile water was added to each well and incubated for 30 min at 37 °C as a measure of microbial growth. After incubation with MTT(3-[4,5-dimethylthiazol-2-yl]-2,5-diphenyltetrazolium bromide), the solution in the well remained clear when microbiological growth was prevented. The test is carried out in accordance with the Gulluce *et al*. [38] procedure with a few minor modifications utilizing the microplate dilution technique (96 wells) with a final volume in each microplate well of 100 µL. Mueller-Hinton broth (MHB), 100 µL, was divided among the second through the twelfth test wells for sensitivity testing.

The stock solution of the extract was created in the first microplate well by combining all of the extracts with 10 percent DMSO (MHB for bacteria) to achieve a final concentration of 25 mg/mL. Then 100 liters of scalar dilutions were transported from the first to the twelfth. The bacterial suspension was then added to each well, replacing 10 mL of the suspension, resulting in final inoculum concentrations of 106 CFU/mL. The antibacterial activity was measured at concentrations ranging from 0.097 to 25 mg/mL. The eleventh well served as a positive control for the development of microorganisms, the twelve well served as a negative control since it contained 10 percent DMSO/MHB without extract, and the tenth well served as a sterile medium. The plates were then covered with sterile plate covers and kept incubating for 24 hours at 37°C. The MTT incubation resulted in no microbiological growth, and the solution in the well remained clear.

2.4. Anticorrosion Activity of Origanum Majorana L (OML-EO).

2.4.1. Preparation of samples.

Ferrous steel is the substance employed in this experiment as the working electrode for electrochemical studies. The used steel coupons have a percent composition (wt.%) of 98.38 percent Fe, 0.28 percent C, 1.25 percent Mn, 0.05 percent S, and 0.04 percent P. Before each test, coupons were polished with emery paper (ranging in grade from 200 to 2000), washed with distilled water, and air dried.

2.4.2. Preparation of electrolytes.

Strong hydrochloric acid (37 percent) was diluted with distilled water to produce the potent solution used in this investigation, 1 M HCl. Concentrations of OML-EO extract ranging from 0.2 to 0.5 g/L were tested. It is necessary to mention that in terms of cost-benefit analysis, the studied inhibitor was prepared without using expensive solvents or any other further cost step; essential oil needs only available acidic media and mixing for 3 h to obtain the homogenous electrolyte medium.

2.4.3. Electrochemical monitoring.

Electrochemical studies, including potentiodynamic polarization curves and electrochemical impedance spectroscopy (EIS) were performed using platinum as the counter electrode, ferrous steel as the working electrode, and a saturated calomel electrode (SCE) as the reference electrode. The PGZ 100 Potentiostat/Galvanostat, which was operated by a computer and used in conjunction with the "Volta Master 4" software to enable the interpretation of experimental data, was used to record all experiments. The EC-Lab program was then used to retrieve the electrochemical parameters.

Before testing, the electrochemical system was stabilized for 30 minutes to establish a steady-state corrosion potential (E_{corr}). The anodic and cathodic polarization curves (PC) were continuously swept from -800 mV to 0 mV at a rate of 0.5 mV/s. Software data for corrosion current density (i_{corr}) and corrosion potential (E_{corr}) were acquired, and the following equation (3) was used to compute inhibition efficiency (η_{Taf}) for various inhibitor doses:

$$\eta_{Taf}\left(\%\right) = \frac{i_{cor}^0 - i_{cor}}{i_{cor}^0} \times 100 \tag{3}$$

where i_{cor}^0 and i_{cor} are the corrosion current densities of Ferrous steel in the non-existence and existence of (OML-EO), respectively.

The EIS tests were conducted using (peak to peak) alternating amplitude signals of 10 mV in a frequency range of 100 kHz to 100 mHz under the identical circumstances as the polarization curve plot. It was done by plotting the EIS diagrams using the Nyquist representation. Investigating the values of the double-layer capacitance (C_{dl}) and polarization resistance (R_P) from these plots allowed for the calculation using equation (4) of the inhibitory efficiency (EIS) for each (OML-EO) concentration using:

$$\eta_{EIS}\left(\%\right) = \frac{R_p^i - R_p^0}{R_p^i} \times 100 \tag{4}$$

where R_p^i and R_p^0 are the polarization resistance values of Ferrous steel in the existence and non-existence of OML-EO, respectively.

2.4.4. Surface imaging.

Scanning Electron Microscopic investigations were carried out on the prepared samples by JEOLJSM-IT 100. In both the non-existence and existence of the OML-optimal EO's concentration, images were captured on samples submerged for 48 hours in 1 M HCl using an accelerating voltage of 20 kV [28].

2.4.5. UV-liquid spectroscopy.

UV-Visible absorption spectra were conducted in 1 M HCl solution with the inclusion of 0.5 g/L of OML-EO before and after dipping the ferrous steel specimen for 6 hours. Spectral monitoring was undertaken in the wavelength range of 200-800 nm using a UV spectral analyzer of type (UV-730, Jasco).

2.4.6. DRX Analysis.

In order to confirm the formation of a productive film by the inhibitor molecule OML-EO on ferrous steel after a 6h immersion in 1 M HCl. The exposed part was removed and dried and submitted to an analysis using a Shimadzu 6100 diffractometer, controlled at 40 kV and 30 mA. The Cu Kα with a wavelength of 1.541838 Å. was used for measurements in an angular range of 4°< θ <110° at room temperature.

2.4.7. DFT and MDO information.

Using the DFT technique in the aqueous phase, we attempted to investigate the mode of action of the new TRO on the Fe- steel surface [39]. A correlation between TRO's calculated experimental inhibitory efficacy and the chemical reactivity indices was also made due to this

theoretical addition [40]. The Gauss.09 software package at the DFT/B3LYP/6-31G (d, p) has optimized the examined compound's molecular structure to its final shape [41].

The electrons that were moved from the occupied orbitals of organic molecules to the vacant orbitals of the metal surface «ΔN110» included the ELUMO, EHOMO, global electronegativity, global hardness, and the electrons. With Φ = (Fe110) = 4.82 eV, the work function (Equation 8) explains the theoretical value of χ in Fe (110) and represents the metallic bulk ((ηFe110) = 0 eV) [42].

$$\Delta E_{gap} = \left(E_{LUMO} - E_{HOMO} \right) \tag{5}$$

$$\chi = \frac{1}{2} \left(E_{LUMO} + E_{HOMO} \right) \tag{6}$$

$$\eta = \frac{1}{2} \left(E_{HOMO} - E_{LUMO} \right) \tag{7}$$

$$\Delta N_{110} = \frac{\chi_{Fe_{110}} - \chi_{inh}}{2 \left(\eta_{Fe_{110}} + \eta_{inh} \right)} = \frac{\Phi - \chi_{inh}}{2\eta_{inh}} \tag{8}$$

Using molecular dynamics, the TRO/Fe (110) system's interaction is investigated (MDO). This simulation was carried out using the Materials Studio 2016 Forcite module [43,44]. A 6-couche slab model representing an (11×11) unit cell was used in each layer of the simulation box (27.30 * 27.30 * 37.13 Å^3) used to run the interactions for the system under study. By 27.13 Å^3, the built-in simulation box has been empty. The $500H_2O$, $5H_3O^+$, $5Cl^-$, and TRO fill this vacuum. The temperature of the simulated system, which had a temperature of 303 K, was controlled by the Andersen thermostat, NVT ensemble, with a simulation time of 600 ps and a time step of 1.0 fs [45].

3. Results and Discussion

3.1. Phytochemical tests.

3.1.1. Essential Oil Yield and Composition.

Hydrodistillation of the aerial parts of O. Majorana L. resulted in pale yellow color oils and a wet smell with a significant yield surrounding 1.92%. This resulting oil yield obtained is higher than reported by some authors [46–48]. Furthermore, Makrane et al. [49] have found a yield of 1.06%(plant grown in Errachidia of Morocco). Whereas similar to the yield of 1.86% obtained by Semiz et al. [50]. Table 1 reports the percent composition of the essential oil, showing that the major components of O. Majorana L. are terpene-4-ol (39.59%), α-terpineol(14.55%), Sabinene hydrate(7.02%) and p-Cymene (4.71%).

Table 1. Composition of oil extracted from*Origanum Majorana L.* of Errachidia region.

	Compounds	Time (mn)	Percentage (%)
1	α-Thujene	11.12	0.17
2	α-Pinene	11.29	0.22
3	Sabinene	11.99	1.22
4	β-Pinene	12.10	0.12
5	β -myrcene	12.18	0.26
6	α-Terpinene	12.73	0.55
7	p-Cymene	12.88	4.71
8	Limonene	12.95	0.42
9	β-Phellandrene	12.99	0.42
10	Eucalyptol	13.03	0.51

	Compounds	Time (mn)	Percentage (%)
11	γ-Terpinene	13.43	1.58
12	α-Terpinolen	13.94	0.55
13	Linalool	14.05	2.41
14	Sabinene hydrate	14.18	7.02
15	p-Menth-2-en-1-ol	14.51	3.08
16	trans-4-Thujanol	14.62	0.39
17	p-Menth-2,8-dien-1-ol	14.87	2.06
18	Terpinen-4-ol	15.55	39.59
19	P-Cymen-8-ol	15.06	0.07
20	α-terpineol	15.69	14.55
21	trans-p-Menth-1-en-3-ol	15.75	0.78
22	cis-p-Menth-1-en-3-ol	15.87	1.44
23	5-isopropenyl-2-methyl-7-oxabicyclo[4.1.0]heptan-2-ol	16.12	0.54
24	Linalyl acetate	16.61	1.28
25	1-trans-Ascaridol glycol	16.81	2.29
26	geranyl acetate	17.04	1.20
27	Caryophyllene	17.48	1.1
28	Alloaromadendrene	17.85	0.35
29	humylene	19.20	0.29
30	ledol	20.98	1.84
31	(-)-Spathulenol	20.98	0.87
32	Caryophyllene oxide	21.75	0.14
33	α-Cadinol	21.62	0.61
34	Chlorpyrifos	22.60	0.20
	Total		92.83
	Monoterpene hydrocarbons		10.73
	Oxygenated monoterpene		76.70
	Sesquiterpene hydrocarbon		1.74
	Oxygenated Sesquiterpene		3.66

The chemical profiling of different components of O. Majorana L. species has been extensively studied. It has been postulated that the essential oil of O. Majorana L. exists mainly in different chemotype forms [2,51]. The most predominant is terpinene-4-ol as the majority compound and, as in our case, with the difference in their percentages [46,52]. This variation in performance can be attributed to the plant's origin and the climate and soil of each country. The chemical profiles of volatile constituents and their concentrations are the most important variables from plant to plant. They help us expect the antioxidant activity before running the biological tests. Many parameters guide the changeset of compounds and their abundance, manner of extraction [53], time and period of harvesting, and conditions of place [54].

3.1.2. Antioxidant activities of *O. Majorana L.*

Three distinct tests—the DPPH assay, FRAP, and ABTS were employed to assess the materials' capacity to scavenge free radicals. The findings of the essential oil of Origanum Majorana L.'s antioxidant activity are provided in Table 2 and displayed in Figure 1; ascorbic acid served as the techniques' positive control.
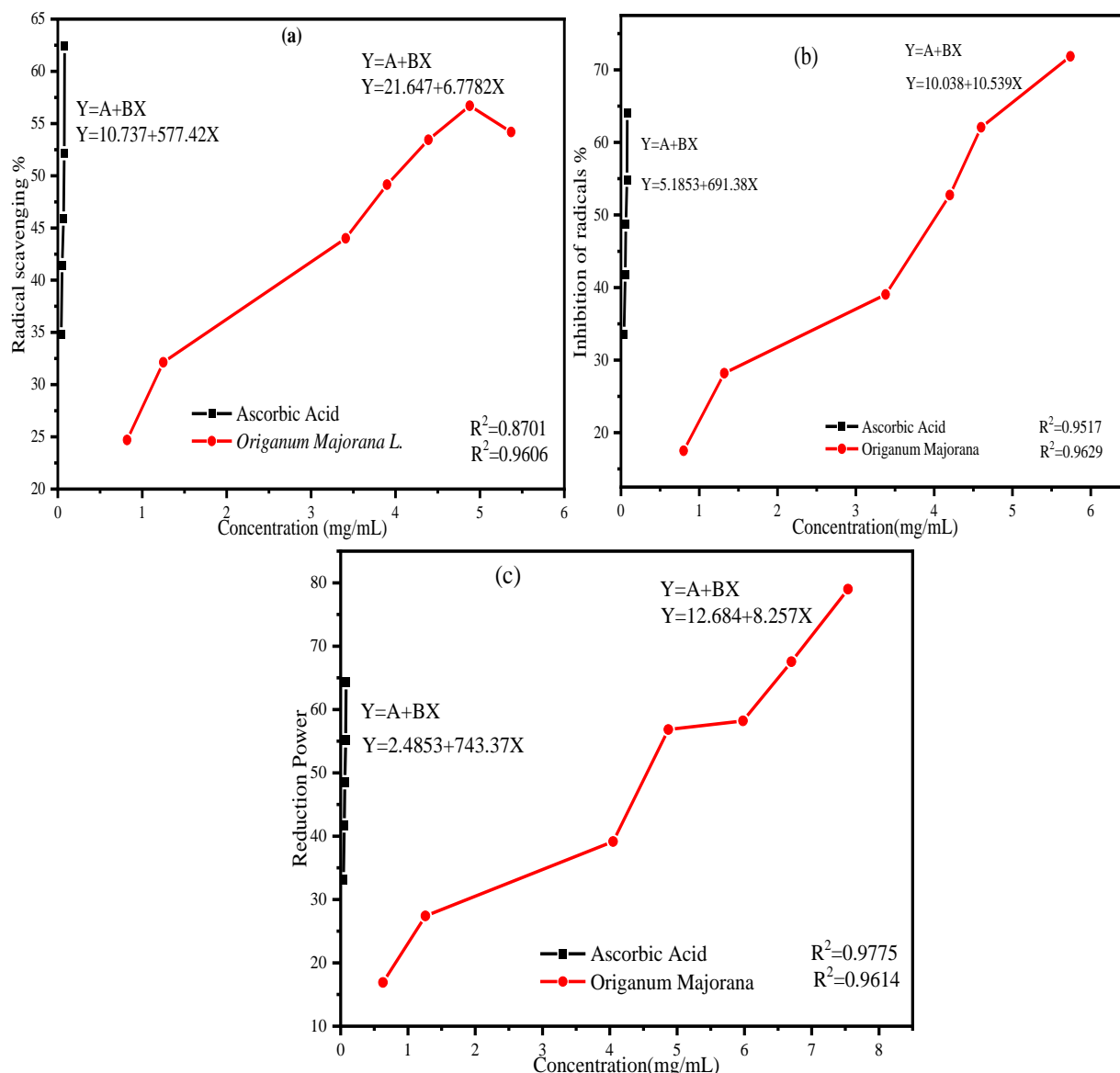
Figure 1. Evolution of percentage inhibition (%) obtained for *OML-EO* by: (**a**) DPPH test, (**b**) ABTS test, (**c**) FRAP Test.

DPPH assay exposes an IC50 of 4.001±0.010 mg/mL. This value seems close to the work prepared by Khadhri *et al*. presenting an IC50= 2.1 mg/mL [55], an author study the Salha *et al*. [56] obtained an IC50 = 0.418 mg. Essentially, *Origanum Majorana* L. bioactive constituents combine with the stabilized free radical, 1,1-diphenyl-2-picrylhydrazyl, representing a dark purple color and converting it to 1,1-diphenyl-2-picrylhydrazine with a yellow discoloration. The decolorization level shows the essential oil's free radical scavenging ability.

ABTS method was so lower in terms of the half minimal inhibitory. An IC50 of 5.439±0,046 mg/mL is considered in agreement with the previous test of DPPH. Both tested methods, DPPH and ABTS assays, are established on the transfer of electrons and protons; they include several reaction mechanisms [57].

The antioxidant property of O. Majorana L. has presumably been associated with a significant proportion of the class of oxygenated monoterpenes. In particular, the major constituent, terpin-4-ol [58,59].

FRAP also shows a respectful ability with an IC50 = 4.518±0.031 mg/mL; the third manner was in correlation with the previously tried methods during this work. Reported studies

show a strong value of IC50= 1.4±0.03 mg/mL [55]; with increasing Origanum Majorana L. concentrations, the decrease of free radicals ranged from 18.11 % to 83%. The three methods showed considerable antioxidant activity, and they agreed. The results are pretty close.

Table 2. Antioxidant activity of the essential oil of *Origanum Majorana L.*

	DPPH	ABTS	FRAP
IC$_{50}$ (mg/mL)	4.001±0.010	5.439±0.046	4.518±0.031
Ascorbic Acid	0.011±0.004	0.064±0.009	0.063±0.003

Data are expressed as mean, standard deviation (n=3), and different letters in the same row represent significant differences at P < 0.05.

3.1.3. Antimicrobial activity.

Several works showed the antibacterial efficacy of essential oil from the plant. An investigation of previous research shows that many studies listed the antibacterial potential of O. Majorana L. against Gram-positive and Gram-negative bacteria.

The result of the antibacterial activity of the OML-EO is presented in Table 3 and Figure 2. Gram-positive bacteria were more negatively affected by the OML-EO than gram-negative bacteria. It was effective against all the tested microorganisms.

Table 3. Antimicrobial activities of the OML-EO.

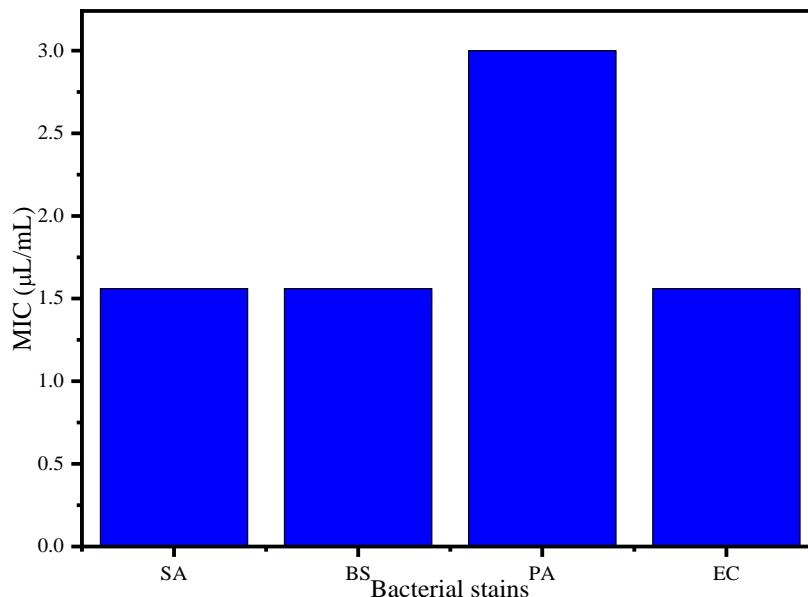| Strains	Minimum inhibitory concentration (MIC) (µL/mL)
Staphylococcus aureus	1.560
Bacillus subtilis	1.560
Pseudomona aeruginosa	3.125
Escherichia coli	1.560

Figure 2. Percentage of antibacterial activity of *OML-EO.*

The MIC observed from the OML-EO is 1.56-3.125 µL/mL. As a result, the plant extracts were efficient against the test bacterium. The bacteria (Pseudomonas aeruginosa) showed a higher MIC = 3.125 µL/mL against tested bacterial strains.

According to the results obtained from the testing we observe a better impact on *Staphylococcus aureus*, *Bacillus subtilis*, and *Escherichia coli* with a (MIC) value equal to 1.56 µL/mL is very low compared to oliverira [59], which finds a value of 5 µL/mL for a

different type of bacteria. The study by Lima [3] results showed that OMEO exhibits an anti-Staphylococcal activity with a MIC equal to 50 µL/mL.

Much research has been done on the antibacterial study of these strains with the microdilution method using (EO) in mg/mL. It also shows a very strong impact on bacteria from its very low MIC values between 3.125 mg/mL and 0.1 mg/mL.

3.2. Study of anticorrosion of (OML-EO).

3.2.1. Polarization curves.

PC measurement (ES) is fundamental for learning about an electrochemical system. After 30 minutes of stabilization at the potential at 303 K, the perturbations of the ferrous metal in 1 M HCl medium, both with and without OML-EO, were undertaken (see Figure 3).
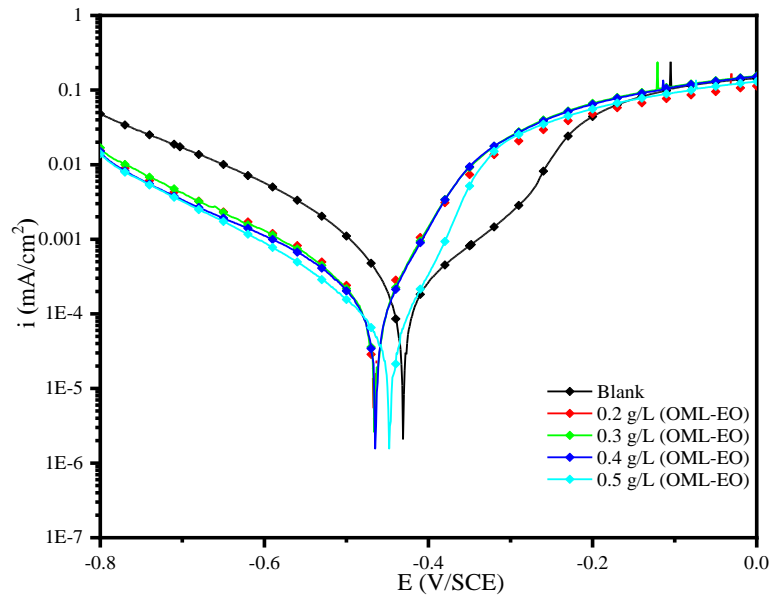

Figure 3. Tafel graph for Ferrous steel in different concentrations of OML-EO in 1 M HCl.

Figure 3 shows the anodic and cathodic polarization curves for the ferrous metal in an acidic solution without and with various chemical concentrations of OML-EO. The electrochemical parameters obtained from the (EC) system studied, namely corrosion current density (icorr), corrosion potential (Ecorr), and Tafel's cathodic coefficient (βc), as well as the protective efficiency (ηTaf) were tabulated in Table 4.

Table 4. (EC) parameters of Fe-steel in 1 M HCl at 303K containing different concentrations of OML-EO.

C. (g/L)	E_{corr} (mV/SCE)	i_{corr} (µA /cm^2)	- β_c (mV/dec)	β_a (mV/dec)	η_{Taf} (%)
Blank	-430.7	617	189	145	-
0.5	-447.3	36	81	46	94
0.4	-464.3	80	90	52	87
0.3	-465.2	94	97	59	85
0.2	-465.9	110	99	63	82

As can be observed, the inclusion of OML-EO in the electrolyte displaced the Ecorr of the Ferrous steel to the negative direction. This can be attributed to the cathodic reaction's kinetics being slower due to the existence of OML-EO. So, from these outcomes, OML-EO can be interpreted as having diminished the corrosion current density (icorr) of the ferrous steel, which indicates that the OML-EO delayed the corrosion rate of Ferrous steel samples in corrosive solution [60–63]. Furthermore, it can be viewed that the protective efficacy ηTaf (%)

of the extract rises with augmentation of OML-EO, up to an optimal concentration of 0.5 g/L and reach a maximum value (94%) as obtained in previous studies carried out by the use of Origanum Majorana as inhibitor [32,33]. Additionally, it should be noted that the OML-EO can be classified as either cathodic or anodic depending on the direction of displacement when the potential corrosion difference between it and the reference solution is larger than 85 mV [15,64]

As a result, the corrosion potential (Ecorr) of Ferrous steel was shifted below 85mV, indicating that the OML-EO product exhibits mixed inhibition effects.

3.2.2. Electrochemical impedance spectroscopy.

To better understand the reaction's mechanism at the Electrolyte-Steel interface, the EIS technique was employed to examine the corrosion inhibition processes. Nyquist plots of the Fe-metal embedded in the corrosive HCl solution, without and with different concentrations of OML-EO, are presented in Figure 4.
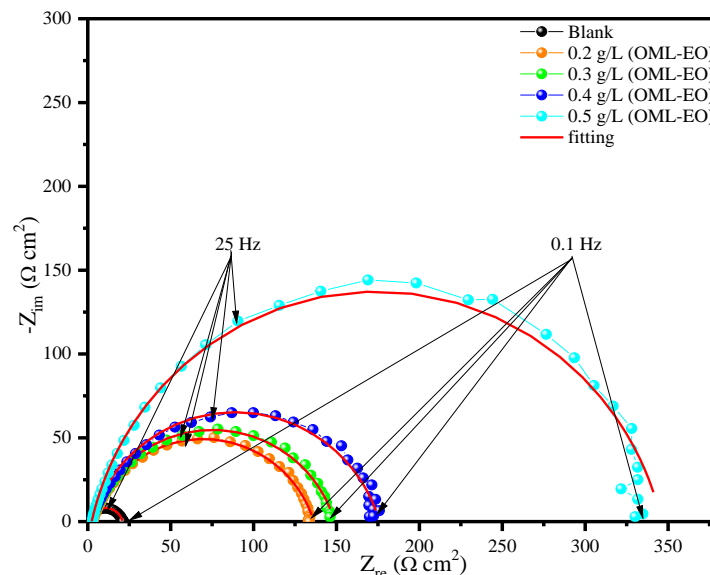

Figure 4. Nyquist plot for Ferrous steel in different concentrations of OML-EO in 1 M HCl.

The Nyquist plots at first sight display only a single depressed capacitive loop, which points out that the corrosion of the Fe-steel tested can be controlled by the charge transfer process. Also, at the electrode's interface, capacitance dispersion occurs, which is strongly dependent on the surface condition of the electrode, its roughness, its degree of polycrystallinity, and also on the adsorption of ions [63,65]. The impedance is characterized by a deviation from the ideal capacitive behavior, which is represented empirically by a constant phase element (CPE), which can be expressed using the following equation (9) [66]:

$$Z_{CPE} = Y_0^{-1} \times (j\omega)^{-n} \tag{9}$$

where ω is the angular frequency in rad s^{-1} ($\omega = 2f$), Y_0^{-1} is a CPE constant, n is a CPE exponent that represents the working electrode's interface surface features, $j^2 = -1$ is the imaginary number, and f is the frequency in Hz [67], the double-layer capacitance has been calculated by the use of equation (10):

$$C_{dl} = Q(\omega_{max})^{n-1} \tag{10}$$

where Q is the constant phase element and $\omega max = 2fmax$ is the angular frequency at the greatest value of the imaginary section of the impedance spectrum (CPE).

Therefore, the simplest electrical equivalent that has been used to describe the present (EC) interface to extract the necessary parameters for understanding the studied system is only the following circuit with a one-time constant which consists of solution resistance (Rs), polarization resistance (Rp) and double-layer capacitance (Cdl) (Figure 5).

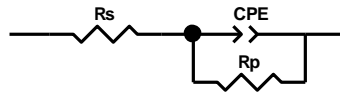**Figure 5.** Equivalent Electrical circuit for fitting the EIS experimental data.

The impedance parameters recorded from the fitting of diagrams and η_{EIS}% are presented in Table 5.

Table 5. EIS parameters in the non-existence and in the existence of the (OML-EO) at diverse concentrations.

C (g/L)	R_s (Ω cm^2)	R_p (Ω cm^2)	Q (μs^n Ω^{-1} cm^{-2})	n	C_{dl} (μF cm^{-2})	Chi squared	η_{EIS} (%)
HCl	0.441	20.6±0.6	507.7±0.2	0.8504±0.0061	227	1×10^{-4}	-
0.5	2.361	343.8±0.9	106.1±0.1	0.8578±0.0014	61.28	2×10^{-3}	94
0.4	2.014	174.0±1.1	132±0.1	0.8199±0.0032	57.62	3×10^{-3}	88
0.3	1.906	147.0±1.2	150.6±0.2	0.8146±0.0032	63.27	5×10^{-3}	86
0.2	2.685	134.0±1.1	159.8±0.2	0.8081±0.0058	64.14	2×10^{-4}	84

The impedance spectra allow the extraction of the parameters listed in Table 5. As shown, the protective efficiency increases to a maximum value of 94%, and the polarization resistance R_p is improved from 20.57 to 343.8 Ω cm^2. As a result, the rise in these latter values suggested that an OML-EO adsorption coating had developed on the Fe-steel substrate, delaying the transfer of charge [68,69]

With an increase in OML-EO concentration of up to 0.5 g/L, the value of the double-layer capacitance (C_{dl}) reduces from 227 to 61.28 μF cm^{-2}. A decrease in the film's local dielectric constant, an increase in the electrical double layer's thickness, or both concurrently occurring factors may be to blame for a decrease in the capacity (C_{dl}) [70].

Therefore, the following equation (11) relates the electrical double layer's thickness to C_{dl} [71]:

$$C_{dl} = \frac{\varepsilon_0 - \varepsilon_r}{A} \tag{11}$$

where A is the effective surface area, ε_r is the relative dielectric constant, and ε_0 is the dielectric constant.

Consequently, the results showed high agreement between the impedance study's and the polarization measurement's results for the corrosion inhibition efficiency.

3.2.3. Temperature effect.

The Tafel tests were performed in the temperature range of 303-333 K, as part of the evaluation of OML-EO adsorption and activation variables of the Ferrous metal oxidation process in an acidic solution without and with 0.5 g/L of OML-EO. The findings are resumed in Figure 6 and Table 6.
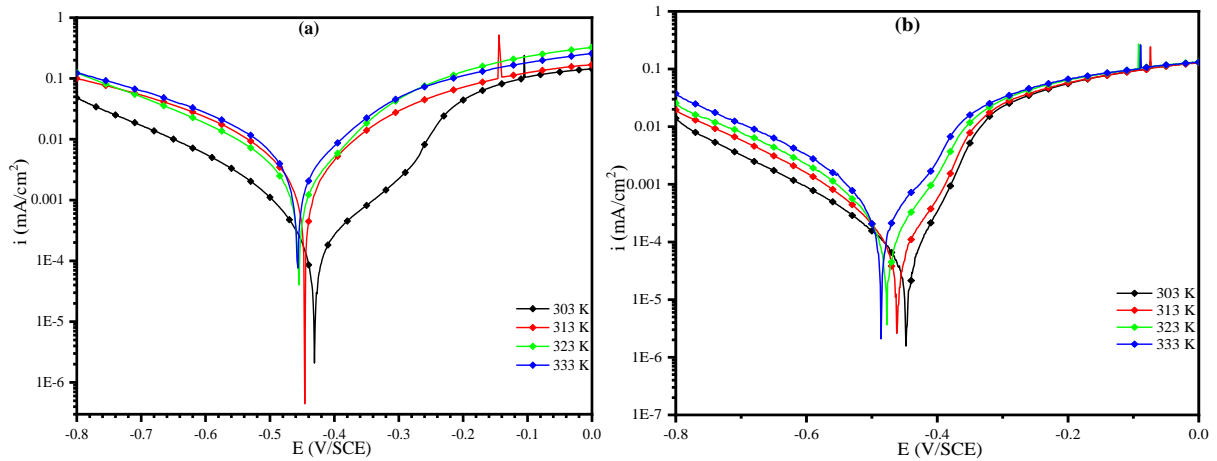
Figure 6. Polarization curves of Fe-steel in 1 M HCl (a) -without OML-EO, (b): with OML-EO at different temperatures.

Table 6. Corrosion parameters of Fe-steel of 1 M HCl + 0.5 g/L OML-EO at different temperatures.

T (K)	i_{corr} ($\mu A/cm^2$)		$\theta = \eta_{Taf}/100$	η_{Taf} (%)
	HCl 1 M	OML-EO		
303	617	36	0.9416	94
313	716	137	0.80	80
323	2073	560	0.72	72
333	2076	856	0.58	58

In fact, the temperature factor is considered an essential parameter to measure the degree of oxidation. To do this, we investigated the effects of a temperature range between 303 and 333 K, the existence or non-existence of OML-EO, and the influence of the extract oil's protective properties [72]. On the other hand, it seems that in an aggressive medium, the protective capacity has decreased with temperature, going from 94% to 58%, while the corrosion current density has increased. This can probably be explained by the desorption of OML-EO molecules [72,73].

Therefore, the following relation (12) may be used to get the activation energy (E^*) using Arrhenius patterns for the corrosion rate (i_{corr}) of ferrous steel, as shown in Figure 7:

$$i_{corr} = A\exp\left(\frac{-E^*}{RT}\right) \tag{12}$$

where R is the universal gas constant (8.314 J/mol K), T is the absolute temperature (K), and A is the frequency factor.
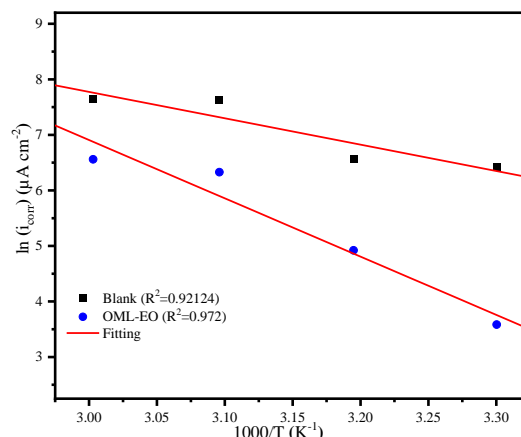

Figure 7. Arrhenius plot for steel in 1 M HCl solution with 0.5 g/L of OML-EO present and absent.

An alternative form of Arrhenius equation (13) is the transition-state equation:

$$i_{corr} = \frac{RT}{Nh} \exp\left(\frac{-\Delta H^*}{RT}\right) \exp\left(\frac{\Delta S^*}{R}\right) \qquad (13)$$
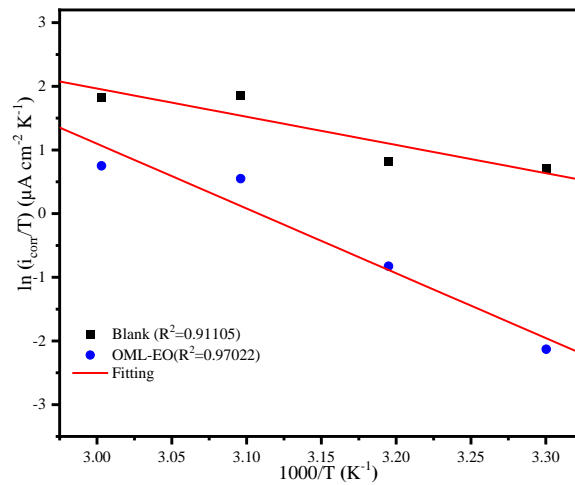

Figure 8. The plot shows the transition states for steel in 1 M HCl in the non-existence and existence of 0.5 g/L of vc OML-EO.

From the data in Table 7, it is noticeable that the E^* value of the solution comprising 0.5 g/L of OML-EO in our case has risen with respect to the standard solution, thus evincing strong adsorption of OML-EO molecules on the ferrous metal surface [74].

Table 7. Activation parameters of the dissolution of Ferrous steel in 1M HCl in the non-existence and existence of 0.5 g/L of OML-EO.

C (g/L)	E^* (kJ/mol)	ΔH^* (kJ /mol)	ΔS^* (J mol K^{-1})
Blank	39.80	37.00	-70
0.5	87.24	84.60	65

The range of E^* values (39.8 and 87.24 kJ/mol), proves that the adsorption of OML-EO is a physical type. Furthermore, based on equation (12), the corrosion rate is impacted by E^* and A. This is apparent from the data below that the value of these parameters is higher when OML-EO was added compared to the standard solution. The diminished corrosion rate with the concentration of OML-EO seems to propose that E^* [75,76]. In contrast, the figure below (Figure 8) presents a graph of ln (i_{corr}/T) as a function of 1000/T. Line graphs are derived with a slope, the enthalpy of activation (ΔS^* J mol K^{-1}), and from the intercepts of the log(i_{corr}/T) axis, the values of the entropy of activation (ΔS^* J mol K^{-1}) were computed and are listed in Table 7.

However, the positive values of ΔH^* (kJ/mol) are indicative of the endothermic character of the Ferrous steel dissolution process. The augmentation of ΔH^* with the enhancement of OML-EO concentration discloses that the diminution of the corrosion rate of Ferrous steel is predominately controlled by the kinetic parameters of the activation process [77]. We remark that the values of E^* are superior to the analogous values of ΔH^*, which points out that the degradation procedure consisted of a gaseous reaction, simply the evolution of hydrogen.

With respect to the activation entropy (ΔS^*), the discussion of the results in Table 7 demonstrates that the corroding metals are ordered in order of importance. Indeed, the arrangement of the attacked metallic surface in the rate-determining phase is a result of the improved formation of complexes. (Negative sign of (ΔS^*) versus the activation step against a pronounced disorder (the positive sign of (ΔS^*) in the existence of OML-EO. Therefore, the latter is involved in a dissociation-type activation process [78]. Besides, the observed augmentation of (ΔS^*) suggests the replacement of water molecules during the adsorption of OML-EO on the ferrous-steel surface [78,79].

3.2.4. Scanning Electron Microscopy (SEM).

In purpose is to identify the nature of the adsorbed products and the morphology of the film formed on the metal studied compared to the steel dipped in the solution without the addition of OML-EO. The (SEM) images of the Ferrous-steel surface having a diameter of 1 cm^2 was exposed in a solution of 1 M HCl for 48 hours in the non-existence and the existence of the optimal concentration of the studied product of 0.5 g/L OML-EO, and are presented respectively in Figure 9.
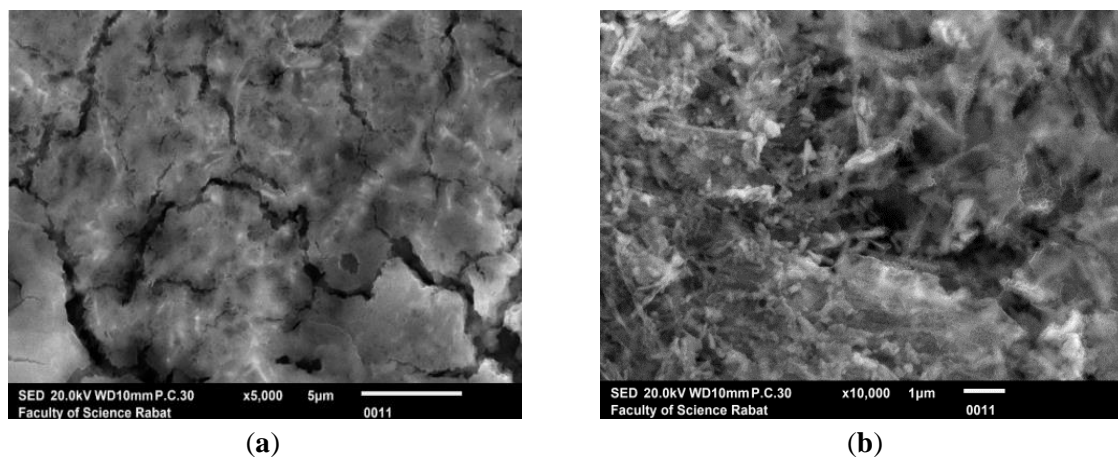

(**a**)   (**b**)

Figure 9. SEM image of Fe-steel surface after 48 hours of (**a**) immersion in 1 M HCl solution alone, (**b**) immersion in 1 M HCl with 0.5 g/L of OML-EO.

The image of the surface of the Ferrous metal dipped at 303 K in 1 M HCl alone (Figure 9-a) clearly shows the existence of corrosion points on the parts submerged in the acid medium. These samples have been corroded decisively, indicating the existence of layers of rust and the accumulation of corrosion products on the surface of the metal.

We note from the SEM the existence of 0.5 g/L of inhibitor (Figure 9-b), and the non-existence of corrosion traces on the samples tested in the solution. The above phenomenon indicates that OML-EO offers better protection against corrosion in a hydrochloric medium, confirming the results obtained by electrochemical measurements.

3.2.5. UV-liquid spectroscopy.

Figure 10 displays UV-vis absorption spectra from 1 M HCl solution containing 0.5 g/L of OML-EO before and after 6 hours of immersion of ferrous steel to confirm the potential of the creation of OML-EO-Fe complex.
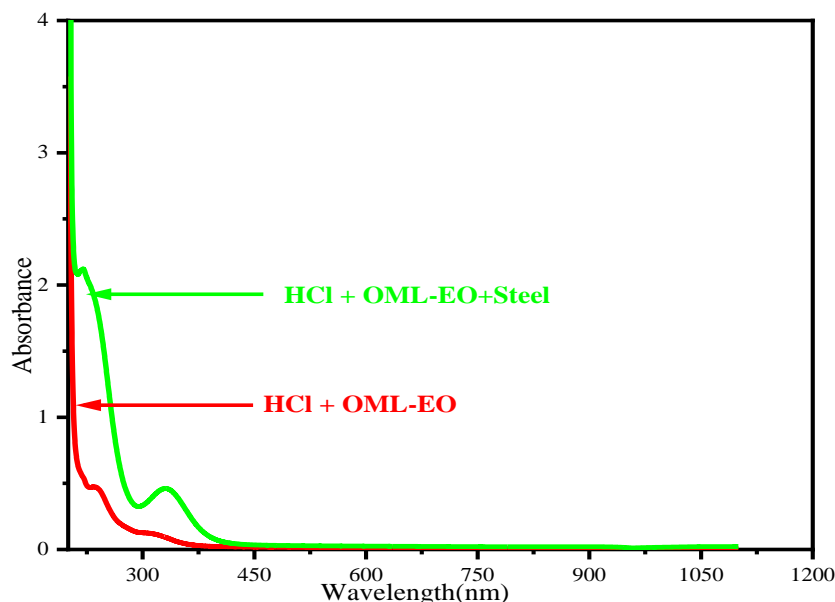
Figure 10. UV spectra without and with the intervention of OML-EO in a solution containing Fe-steel in HCl.

Absorption spectra of OML-EO in 1 M HCl prior to Fe-steel dipping revealed weak adsorption of the inhibitor characterized by two short wavelength absorption bands. The first less intense peak at 330 nm can be assigned due to the n→ π* electronic transition [80], and the second peak of average absorbance occurred at 242nm is due to the $\pi \to \pi*$ transitions of the aromatic ring present in the main compound [42,81].

The spectra also noted that the absorbance values after immersion in the Fe steel were higher than those seen for the solution before immersion [82]. Furthermore, we pointed out the appearance of two distinctive absorbance peaks in the same range (200-400 nm). In comparison, the most intense absorbance peak appears at 218 nm, corresponding to a transition ($\pi \to \pi*$). The second peak at 330 nm is associated with the absorption of functional groups contained in the inhibitor molecules ($n \to \pi*$) [82]. It was also observed that there is a change in the position of the absorption maximum.

Earlier research reported that the offset of the wavelength with the change in absorbance is caused by the formation of a complex between the inhibitor and the metal ion in the solution [81,83]. This fact permits us to conclude that there is a possibility of forming a complex between the extract's main molecule and the Fe-ion, which can contribute to the inhibitory action. These results have already been confirmed by studies in the literature [42,81,82,84].

3.2.6. X-ray diffraction analysis.

After an analysis of Figure 11, it can be noted that the comparison between the diffraction patterns shows no significant differences between the XRD pattern of the uncorroded and corroded surfaces after exposure to 1 M HCl + 0.5 g/L OML-EO. The plot displays no indication of film formation on the surface of the Fe-steel electrode. In addition, the high peak intensity observed around 45° at 2θ is related to the Fe phase, and the peaks related to iron oxides are not observed.

In the case of OML-EO, the lower peak intensity points to binding between the Fe-steel and the OML-EO inhibitor molecules, probably due to the formation of metal complexes [85,86].
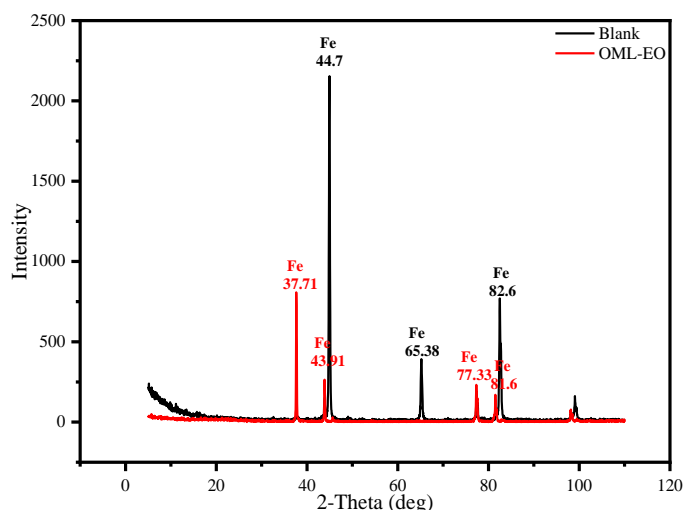
Figure 11. XRD spectrum of Fe-steel corrosion in the non-existence and existence of OML-EO.

3.2.7. DFT approach.

The reactivity of an organic compound with an anticorrosive property of metal support is theoretically evaluated using the DFT approach [87]. Figure 12 represents the optimized structure and the HOMO§LUMO electron density distributions on the TRO. The structure visualized in Figure 12 shows that this geometry is well stable in space with positive frequencies. The distribution of HOMO and LUMO occupies the entire structure of the optimized compound. This property shows that this species is more reactive with the Fe-surface. Therefore, there will be better protection against corrosive ions located in an acidic environment.
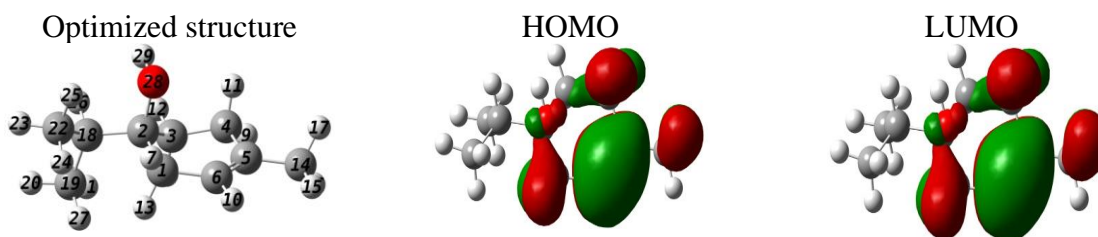

Figure 12. Optimized structure and the FMO electron density distributions.

The overall reactivity descriptors are listed in Table 8. The energies E_{HOMO} and E_{LUMO} measure the level of give and take of the electrons in their relations with the surface of the metal [88]. The high value of E_{HOMO} (-6.043 eV) and the minimum value of E_{LUMO} (1.034 eV) indicate that the tested compound has high chemical reactivity. Consequently, this reactivity is sustained by the minimum value of ΔE_{gap} (7.077 eV) [89]. Electronegativity (χ) and hardness (η) are other descriptors of reactivity in which the minimum value of these two parameters (χ = 2.504 eV, η = 3.538 eV) reflects a high chemical reactivity [90]. The parameter $\Delta N110$ describes the electron donor capacity; a positive value of this descriptor reflects the donor capacity of the inhibitor molecule to vacuum orbitals in the iron surface [90]. In Table 8, we conclude that the TRO is capable of yielding electrons.

Table 8. Chemical reactivity parameters describing the electronic system of TRO.

Descriptors	E_{HOMO} (eV)	E_{LUMO} (eV)	ΔE_{gap} (eV)	χ (eV)	η (eV)	ΔN_{110}
TRO	-6.043	1.034	7.077	2.504	3.538	0.327

It is common knowledge that the reactivity of an inhibitor molecule and the recovery rate of a metal substrate against the corrosion procedure is mostly dependent on the most active sites of this molecule's selectivity (local) [91]. There are two more well-known methods for this purpose, namely the molecular electrostatic potential (MEP) and the Fukui indices (FI) [92]. The topographic distributions of MEP and FI on the structure of TRO are apparent in Figure 12. The red color in this figure represents the electron donor centers (f (-)), while the blue color represents the electron acceptor sites (f (+)) [93]. As observed from Figure 13 and Table 9, the atoms C5 and C6 are the most donor and acceptor sites of electrons simultaneously. These sites may be liable for the inhibitory property of TRO of Ferrous steel in the acidic solution.
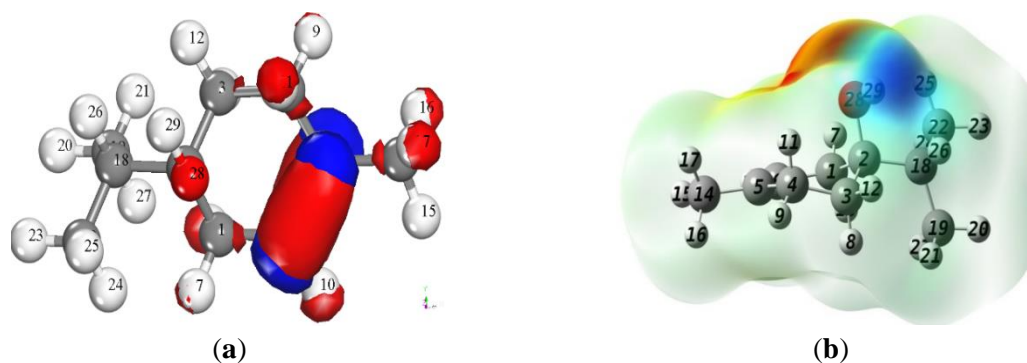

(a)	(b)

Figure 13. Fukui functions (a) and MEP (b) repartitions on TRO structure.

Table 9. Fukui indice sites of TRO.

Atoms	f (-)	f (+)
C (1)	0.030	0.029
C (2)	0.001	0.001
C (3)	0.007	0.007
C (4)	0.028	0.031
C (5)	0.181	0.176
C (6)	0.221	0.206
C (14)	0.039	0.040
C (18)	0.003	0.003
C (19)	0.007	0.007
C (22)	0.004	0.004
O (28)	0.010	0.010

3.2.8. Molecular dynamics ownership (MDO).

In an effort to find a more favorable and stable adsorption configuration, the MDP was used to calculate the ($E_{interaction}$) and binding ($E_{binding}$) energies using equations (14) and (15), respectively, at the interfacial level Fe (1 1 0)/TRO [94].

$$E_{int\,eraction} = E_{total} - E_{surface+solution} - E_{inhibitor} \qquad (14)$$

$$E_{binding} = -E_{int\,eraction} \qquad (15)$$

Figure 13 displays the adsorption configuration of TRO on the atomic Ferrous simulated. Through the visual analysis of Figure 14, we notice that the simulated molecule adsorbs itself through its structure in order to cover a large part of the atomic surface of steel. This adsorption behavior indicates that TRO performs as a better inhibitor against the degradation of our substrate [95].

The calculated values of $E_{interaction}$ and $E_{binding}$ are –672.18 and 672.18 kJ mol^{-1}, respectively. The negative value of $E_{interaction}$ and the positive value of $E_{binding}$ reveal TRO's spontaneity and strong adsorption process, respectively [96]. This type of adsorption confirms

that the chosen compound carries several active sites dispersed over the whole structure. Therefore, there is better protection of treated steel against corrosive species.
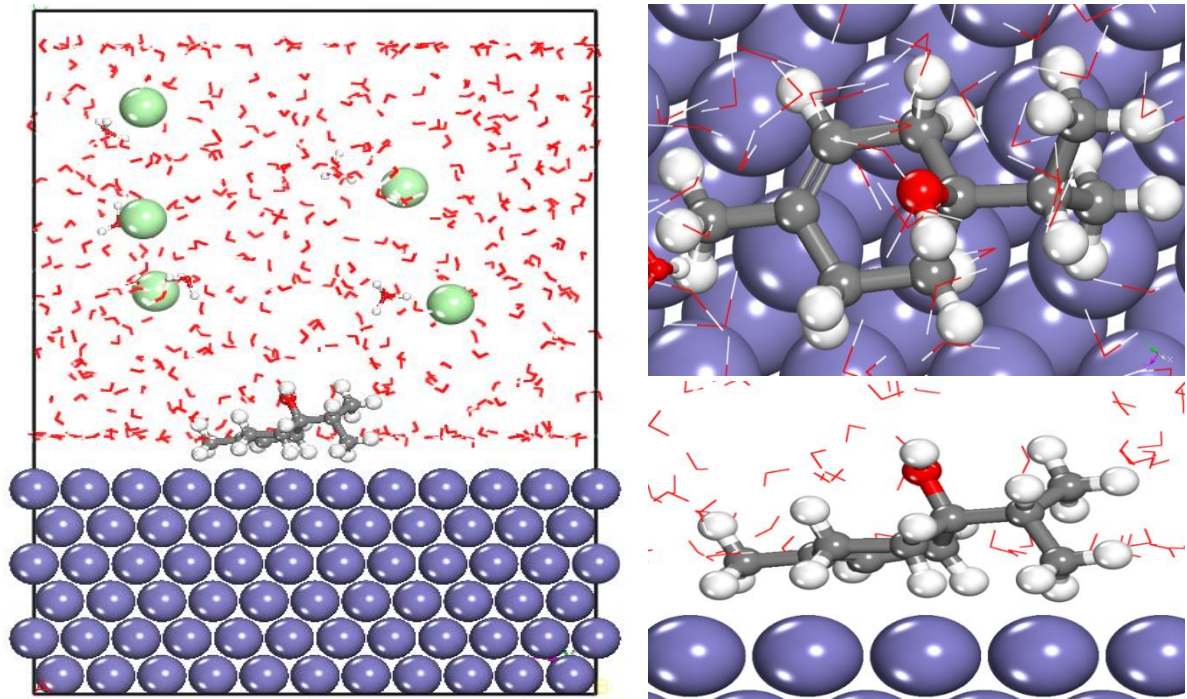

Figure 14. Adsorption aspects of **TRO** on atomic Ferrous.

The radial distribution function (RDF) approach was used to identify the bond distances between TRO and the iron atoms in the first layer (Fe (1 1 0)) [97]. The literature search tells us that if the first peak due to the interaction of species Q with species N presented in the graphical representation of gQN (r) versus the r distance is located between 1 and 3.5 Å, it is assumed that the nature of their interaction is chemisorption, while if the peaks appear at positions superior to 3.5 Å, it is physisorption [98,99]. The RDF findings are shown in Figure 15. This figure makes it clear that the first peak of the RDF produced for the interactions of the TRO with the ferrous surface atoms, g(r)Fe (110)-TRO, has a value of 1.71Å. This chemisorption of TRO on the surface of Fe (1 1 0) promotes the development of a protective layer that serves as a barrier and shields the steel under test from the corrosion process.
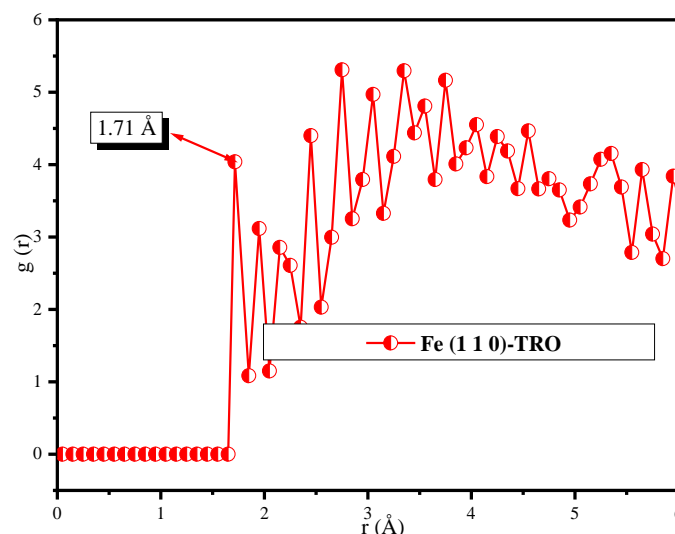

Figure 15. RDF of TRO on Fe.

4. Conclusions

In this work, we shed light on the chemical composition (GC/MS), antioxidant activities, antibacterial activities and anticorrosive activity of the essential oil of OML, and the above analysis and discussion of the experimental results lead to the following main conclusions: The chromatographic analysis (GC/MS) of the OML-EO has proved that it is rich in potentially bioactive compounds with a dominance of terpinene-4-ol (39.59%) and α-terpineol (14.55%); A high antioxidant capacity of OML-EO was confirmed by tests (FRAP, DPPH, and ABTS tests); Based on the above results, the oil is very effective against bacterial strains against Gram-positive (*Staphylococcus aureus, Bacillus subtilis*) and Gram-negative (*Escherichia coli, Pseudomonas aeruginosa*) bacteria, which is validated by a very low MIC; The findings obtained from the PDP curves marked that OML-EO is a mixed-type inhibition; at 0.5 g/L concentration of OML-EO, the electrolyte exhibited an inhibition performance of 94%; The impedance plots of the mild steel revealed that the inhibition efficiency improved with the concentration of the plant extract, and the corrosion process was controlled by the charge transfer and corroborated the PDP measurements; According to the results found from the thermodynamic parameters, it is possible to confirm the formation of a protective film by the adsorption of OML-EO, replacing the initially adsorbed water molecules; The monitoring of the surface morphology using SEM corroborated these results by showing a regular growth of a protective film on the corroded surface, reaching a dense morphology at the optimal concentration, which showed the highest (IE%) under the current working conditions; The UV-visible X-ray examinations gave clear evidence of a complex formation, which may also be responsible for the monitored protection; Quantum chemical parameters obtained from the DFT method showed a good correlation between experimental data and the electronic properties of the major inhibitor compound.

Funding

Acknowledgments

Conflicts of Interest

The authors declare no conflict of interest.

References

1. Enujiugha, V. N.; Talabi, J. Y.; Malomo, S. A.; Olagunju, A. I. DPPH Radical Scavenging Capacity of Phenolic Extracts from African Yam Bean (Sphenostylis stenocarpa). *Food and Nutrition Sciences* **2012**, *3*, 7-13, http://dx.doi.org/10.4236/fns.2012.31002.
2. Charai, M.; Mosaddak, M.; Faid, M. Chemical Composition and Antimicrobial Activities of Two Aromatic Plants : Origanum majorana L. and O. compactum. *Journal of Essential Oil Research* **1996**, 37–41, https://doi.org/10.1080/10412905.1996.9701036.
3. Lima, J. De; Martins, L.; Daiana, G.; Schneid, I.; Padilha, W.; Maria, A. Antimicrobial activity of essential oils of Origanum vulgare L. and Origanum majorana L. against *Staphylococcus aureus* isolated from poultry meat. *Industrial Crops & Products* **2015**, *77*, 444–450, https://doi.org/10.1016/j.indcrop.2015.09.013.
4. Santana, O.; Andrés, M. F.; Sanz, J.; Errahmani, N.; Abdeslam, L.; González-Coloma, A. Valorization of essential oils from Moroccan aromatic plants. *Natural Product Communications* **2014**, *9*, 1109–1114, https://doi.org/10.1177/1934578x1400900812.

5. Kulisic, T.; Radonic, A.; Katalinic, V.; Milos, M. Use of different methods for testing antioxidative activity of oregano essential oil. *Food Chemistry* **2004**, *85*, 633–640, https://doi.org/10.1016/j.foodchem.2003.07.024.

6. Suhaj, M. Spice antioxidants isolation and their antiradical activity: a review. *Journal of Food Composition and Analysis* **2006**, *19*, 531–537, https://doi.org/10.1016/j.jfca.2004.11.005.

7. Augustyniak, A.; Bartosz, G.; Čipak, A.; Duburs, G.; Horáková, L.; Łuczaj, W.; Majekova, M.; Odysseos, A. D.; Rackova, L.; Skrzydlewska, E.; Stefek, M.; Štrosová, M.; Tirzitis, G.; Venskutonis, P. R.; Viskupicova, J.; Vraka, P. S.; Žarković, N. Natural and synthetic antioxidants: An updated overview. *Free Radical Research* **2010**, *44*, 1216–1262, https://doi.org/10.3109/10715762.2010.508495.

8. Sindhi, V.; Gupta, V.; Sharma, K.; Bhatnagar, S.; Kumari, R.; Dhaka, N. Potential applications of antioxidants–A review. *Journal of Pharmacy Research* **2013**, *7*, 828–835, https://doi.org/10.1016/j.jopr.2013.10.001.

9. Yashin, A.; Yashin, Y.; Xia, X.; Nemzer, B. Antioxidant activity of spices and their impact on human health: A review. *Antioxidants* **2017**, *6*, 1–18, https://doi.org/10.3390/antiox6030070.

10. Roby, M. H. H.; Sarhan, M. A.; Selim, K. A. H.; Khalel, K. I. Evaluation of antioxidant activity, total phenols and phenolic compounds in thyme (Thymus vulgaris L.), sage (Salvia officinalis L.), and marjoram (Origanum majorana L.) extracts. *Industrial Crops and Products* **2013**, *43*, 827–831, https://doi.org/10.1016/j.indcrop.2012.08.029.

11. Vagi, E.; Sinamdi, B.; Rapavi, E.; Hadolin, M.; Vasarhelyine, K. P.; Blazovics, A. Antioxidant Activity of Origanum Majorana L. Herb and Extracts Obtained By Supercritical Co2 Extraction. *Ninth Meeting on Supercritical Fluids* **2005**, 1–6, https://doi.org/10.1021/jf048777p.

12. Ai-Bandak, G.; Oreopoulou, V. Antioxidant properties and composition of Majorana syriaca extracts. *European Journal of Lipid Science and Technology* **2007**, *109*, 247–255, https://doi.org/10.1002/ejlt.200600234.

13. Dhull, S. B.; Kaur, P.; Purewal, S. S. Phytochemical analysis, phenolic compounds, condensed tannin content and antioxidant potential in Marwa (Origanum majorana) seed extracts. *Resource-Efficient Technologies* **2016**, *2*, 168–174, https://doi.org/10.1016/j.reffit.2016.09.003.

14. El Ouasif, L.; Laourayed, M.; Benhiba, F.; Boudalia, M.; El Ghoul, M.; Achour, R.; Bellaouchou, A.; Guenbour, A.; Warad, I.; Zarrouk, A. Experimental and Theoretical Approaches for Interfacial Adsorption of Novel Long Chain Benzimidazolium Derivatives for Mild Steel Protection in 1 M HCl Medium. *Analytical and Bioanalytical Electrochemistry* **2021**, *13*, 12-32.

15. Laourayed, M.; El Moudane, M.; Khachani, M.; Boudalia, M.; Guenbour, A.; Bellaouchou, A.; Zarrouk, A. Thermal, structural and corrosion inhibition performances of a new phosphate glasses on mild steel in HCl medium. *Chemical Data Collections* **2019**, *24*, https://doi.org/10.1016/j.cdc.2019.100305.

16. Boudalia, M.; Bellaouchou, A.; Guenbour, A.; Bourazmi, H.; Tabyaoui, M.; El Fal, M.; Ramli, Y.; Essassi, E.M. Study of Pyrazolo [3, 4-d] pyrimidine Derivative as Corrosion Inhibitor on 904L stainless Steel in Molar H_3PO_4. *Moroccan Journal of Chemistry* **2014**, *2*, 97–109.

17. Boudalia, M.; El Bakri, Y. Echihi. S.; Harmaoui. A.; Sebhaoui, J.; Bellaouchou, A.; Guenbour, A., Tabyaoui, M.; Ramli, Y.; Essassi, E.M.; Electrochemical methods for monitoring the performance of a novel Triazole derivative as a corrosion inhibitor in the acidic medium. J*ournal of Materials and Environmental Science* **2017,** *8*, 2094–2104.

18. Alamiery, A.A. Investigations on Corrosion Inhibitory Effect of Newly Quinoline Derivative on Mil Steel in HCl Solution Complemented with Antibacterial Studies. *Biointerface Research in Applied Chemistry* **2022**, *12*, 1561–1568, https://doi.org/10.33263/BRIAC122.15611568.

19. Boudalia, M.; Fernández-Domene, R.M.; Tabyaoui, M.; Bellaouchou, A.. Guenbour, A.; García Antón, J. Green approach to corrosion inhibition of stainless steel in phosphoric acid of Artemesia herba albamedium using plant extract. Journal of Materials Research and Technology **2019**, *8***,** 5763–5773, https://doi.org/10.1016/j.jmrt.2019.09.045.

20. Laqhaili, A.; Hakiki, A.; Mossaddak, M.; Boudalia, M.; Bellaouchou, A.; Guenbou, A.; Morhit, M. El; Hammouti, B. Effect of lavandula stoechas oil on welded material corrosion in 5.5M H3PO4 solution. *Journal of Chemical and Pharmaceutical Research* **2013**, *5*, 1297–1306,

21. Najem, A.; Sabiha, M.; Laourayed, M.; Belfhaili, A.;. Benhiba, F.; Boudalia, M.; Warad, I.; Bellaouchou, A.; Guenbour, A.; Zarrouk, A. New Green Anti-corrosion Inhibitor of Citrus Peels for Mild Steel in 1 M HCl: Experimental and Theoretical Approaches. *Chemistry Africa* **2022**, 5, https://doi.org/10.1007/s42250-022-00366-9.

22. Rbaa, M.; Benhiba, F.; Hsissou, R.; Lakhrissi, Y.; Lakhrissi, B.; Ebn Touhami, M.; Warad, I.; A.; Zarrouk, A. Green synthesis of novel carbohydrate polymer chitosan oligosaccharide grafted on d-glucose derivative as bio-based corrosion inhibitor. *Journal of Molecular Liquids* **2020**, *322*, 114549, 0167-7322, https://doi.org/10.1016/j.molliq.2020.114549.

23. Salleh, S. Z.; Yusoff, A. H.; Zakaria, S. K.; Taib, M. A. A.; Abu Seman, A.; Masri, M. N.; Mohamad, M.; Mamat, S.; Ahmad Sobri, S.; Ali, A.; Teo, P. Ter Plant extracts as green corrosion inhibitor for ferrous metal alloys: A review. *Journal of Cleaner Production* **2021**, *304*, https://doi.org/10.1016/j.jclepro.2021.127030.

24. Tayebi, H.; Himmi, B.; Ramli, Y.; Zarrouk, A.; Geunbour, A.; Bellaouchou, A.; Zarrok, H.; Boudalia, M.; El

Assyry, A. Experimental and theoretical investigation of 5-(azidomethyl)quinolin-8-ol as a corrosion inhibitor for carbon steel in hydrochloric acid medium. *Research Journal of Pharmaceutical, Biological and Chemical Sciences* **2015**, *6*, 1861–1873.

25. Alrefaee, S. H.; Rhee, K. Y.; Verma, C.; Quraishi, M. A.; Ebenso, E. E. Challenges and advantages of using plant extract as inhibitors in modern corrosion inhibition systems: Recent advancements. *Journal of Molecular Liquids* **2021** , *321*, 114666, https://doi.org/10.1016/j.molliq.2020.114666.

26. Ezzat, A.; Abdel Motaal, S.M.; Amal, S. A.; Sallam, H.B.; El-Hossiany, A.; Fouda, A.S. Corrosion Inhibition of Carbon Steel in 2.0M HCl Solution Using Novel Extract (Pulicaria undulate). *Biointerface Research in Applied Chemistry* 2**022**, *12*, 6415–6427, https://doi.org/10.33263/BRIAC125.64156427.

27. Chaudhary, S.; Tak, R.K. Corrosion Inhibition of Carbon Steel in 2.0M HCl Solution Using Novel Extract (Pulicaria undulate). *Biointerface Research in Applied Chemistry* 2**022**, *12*, 2603–2617, https://doi.org/10.33263/BRIAC122.26032617.

28. Echihi, S.; Hsissou, R.; Benzbiria, N.; Afrokh, M.; Boudalia, M.; Bellaouchou, A.; Guenbour, A.; Azzi, M.; Tabyaoui, M. Performance of methanolic extract of artemisia herba alba as a potential green inhibitor on corrosion behavior of mild steel in hydrochloric acid solution. *Biointerface Research in Applied Chemistry* **2021**, *11*, 14751–14763, https://doi.org/10.33263/BRIAC116.1475114763.

29. Tayebi, H.; Himmi, B.; Ramli, Y.; Zarrouk, A.; Geunbour, A.; Bellaouchou, A.; Zarrok, H.; Boudalia, M.; El Assyry, A. Experimental and theoretical investigation of 5-(azidomethyl)quinolin-8-ol as a corrosion inhibitor for carbon steel in hydrochloric acid medium. *Research Journal of Pharmaceutical, Biological and Chemical Sciences* **2015**, *6*, 1861–1873.

30. Hsissou, R.; Abbout, S.; Benhiba, F.; Seghiri, R.; Safi, Z.; Kaya, S.; Briche, S.; Serdaroğlu, G.; Erramli, H.; Elbachiri, A.; Zarrouk, A.; El Harfi, A. Insight into the corrosion inhibition of novel macromolecular epoxy resin as highly efficient inhibitor for carbon steel in acidic mediums: Synthesis, characterization, electrochemical techniques, AFM/UV–Visible and computational investigations, *Journal of Molecular Liquids* **2021**, *337*, 0167-7322, https://doi.org/10.1016/j.molliq.2021.116492.

31. Hsissou, R.; Abbout, S.; Seghiri, R.; Rehioui, M.; Berisha, A.; Erramli, H. Assouag, M.; Elharfi, A. Evaluation of corrosion inhibition performance of phosphorus polymer for carbon steel in [1M] HCl: Computational studies (DFT, MC and MD simulations), *Journal of Materials Research and Technology* **2020**, *9*, 2691-2703, https://doi.org/10.1016/j.jmrt.2020.01.002.

32. Sobhi, M. Marjoram Extract as Corrosion Inhibitor for Dissolution of Zinc in 1 . 0 M HCl, *International Journal of Corrosion* **2013**, *2013*, http://dx.doi.org/10.1155/2013/763476%0A.

33. Ganash, A.A.Theoretical and experimental studies of dried marjoram leaves extract as green inhibitor for corrosion protection of steel substrate in acidic solution. *Chemical Engineering Communications*. **2018**, *205*, 350-62. https://doi.org/10.1080/00986445.2017.1391096.

34. Tahraoui, A.; El-hilaly, J.; Israili, Z. H.; Lyoussi, B. Ethnopharmacological survey of plants used in the traditional treatment of hypertension and diabetes in south-eastern Morocco (Errachidia province). *Journal of ethnopharmacology* **2007**, *110*, 105–117, https://doi.org/10.1016/j.jep.2006.09.011.

35. Hatano, T., Kagawa, H., Yasuhara, T., Okuda, T. Two new flavonoids and other constituents in licorice root: their relative astringency and radical scavenging effects. *Chemical and pharmaceutical bulletin*. **1988**, *36*, 2090-2097.

36. Re, R.; nicoletta, P.; Proteggente, A.; PannalA, A.; Yang, M.; Rice-Evans, C. Development and characterisation of carbon nanotube-reinforced polyurethane foams. *Free Radical Biology & Medicine* **1998**, *26*, 51.

37. Oyaizu, M. Studies on products of browning reaction. *The Japanese Journal of Nutrition and Dietetics* **1986**, *44*, 307–315.

38. Gulluce, M.; Sahin, F.; Sokmen, M.; Ozer, H.; Daferera, D.; Sokmen, A.; Polissiou, M.; Adiguzel, A.; Ozkan, H. Antimicrobial and antioxidant properties of the essential oils and methanol extract from Mentha longifolia L. ssp. longifolia. *Food Chemistry* **2007**, *103*, 1449–1456, https://doi.org/10.1016/j.foodchem.2006.10.061.

39. El Faydy, M.; Benhiba, F.; Warad, I.; Saoiabi, S.; Alharbi, A.; Alluhaybi, A.A.; Lakhrissi, B.; Abdallah, M.; Zarrouk, A. Bisquinoline analogs as corrosion inhibitors for carbon steel in acidic electrolyte: Experimental, DFT, and molecular dynamics simulation approaches. *Journal of Molecular Structure* **2022**, *1265*, 133389, https://doi.org/10.1016/j.molstruc.2022.133389.

40. Berrissoul, A.; Ouarhach, A.; Benhiba, F.; Romane, A.; Guenbour, A.; Dikici, B.; Bentiss, F.; Zarrouk, A.; Dafali, A. Assessment of corrosion inhibition performance of origanum compactum extract for mild steel in 1 M HCl: Weight loss, electrochemical, SEM/EDX, XPS, DFT and molecular dynamic simulation. *Industrial Crops & Products* **2022**, 187, 115310, https://doi.org/10.1016/j.indcrop.2022.115310.

41. Oubaaqa, M.; Ouakki, M.; Rbaa, M.; Benhiba, F.; Galai, M.; Idouhli, R.; Maatallah, M.; Jarid, A.; Warad, I.; Lakhrissi, B.; Zarrouk, A.; Ebn Touhami, M. Experimental and theoretical investigation of corrosion inhibition effect of two 8-hydroxyquinoline carbonitrile derivatives on mild steel in 1 M HCl solution. *Journal of Physics and Chemistry of Solids* **2022**, *169*, 110866, https://doi.org/10.1016/j.jpcs.2022.110866.

42. EL Hassouni, H.; Elyousfi, A.; Benhiba, F.; Setti, N.; Romane, A.; Benhadda, T.; Zarrouk, A.; Dafali, A. Corrosion inhibition, surface adsorption and computational studies of new sustainable and green inhibitor for mild steel in acidic medium. *Inorganic Chemistry Communications* **2022**, *143*, 109801,

https://doi.org/10.1016/j.inoche.2022.109801.

43. Abouchane, M.; Dkhireche, N.; Rbaa, M.; Benhiba, F.; Ouakki, M.; Galai, M.; Lakhrissi, B.; Zarrouk, A.; Ebn Touhami, M. Insight into the corrosion inhibition performance of two quinoline-3- carboxylate derivatives as highly efficient inhibitors for mild steel in acidic medium: Experimental and theoretical evaluations. *Journal of Molecular Liquids* **2022**, *360*, 119470, https://doi.org/10.1016/j.molliq.2022.119470.

44. Materials Studio, Revision 8.0, Accelrys Inc., San Diego, U. *Modules Tutorials* **2017**.

45. Andersen, H. C. Molecular dynamics simulations at constant pressure and / or temperature Molecular dynamics simulations at constant pressure and / or temperature. *The Journal of chemical physics*, **2007**, *2384*, 2384–2393.

46. Ouedrhiri, W.; Balouiri, M.; Bouhdid, S.; Moja, S.; Chahdi, F. O.; Taleb, M.; Greche, H. Mixture design of Origanum compactum , Origanum majorana and Thymus serpyllum essential oils : Optimization of their antibacterial. *Industrial Crops & Products* **2016**, *89*, 1–9, https://doi.org/10.1016/j.indcrop.2016.04.049.

47. Amor, G.; Caputo, L.; Storia, A. La; Feo, V. De; Mauriello, G.; Fechtali, T. Artemisia herba-alba and Origanum majorana Essential Oils from Morocco. *Molecules* **2019**, *24*, https://doi.org/10.3390/molecules24224021.

48. Alizadeh, A.; Khosh-Khui, M.; Javidnia, K.; Firuzi, O.; Jokar, S. M. Chemical composition of the essential oil, total phenolic content and antioxidant activity in Origanum majorana L. (Lamiaceae) cultivated in Iran. *Advances in Environmental Biology* **2011**, *5*, 2326–2331.

49. Makrane, H.; Aziz, M.; Mekhfi, H.; Ziyyat, A.; Legssyer, A.; Melhaoui, A.; Berrabah, M.; Bnouham, M.; Alem, C.; Elombo, F. K.; Gressier, B.; Desjeux, J. F.; Eto, B. Myorelaxant Activity of essential oil from Origanum majorana L. on rat and rabbit Hanane. *Journal of Ethnopharmacology* **2019**, *228*, 40–49, https://doi.org/10.1016/j.jep.2018.08.036.

50. Semiz, G. Essential oil composition , total phenolic content , antioxidant and antibiofilm activities of four Origanum species from southeastern Turkey. *International Journal of Food Properties* **2018**, *21*, 209–219, https://doi.org/10.1080/10942912.2018.1440240.

51. Muqaddas; Khera, R. A.; Nadeem, F.; Jilani, M. I. Essential chemical constituents and medicina51uses of Marjoram (Origanum majorana L.) – A comprehensive review. *International Journal of Chemical and Biochemical Sciences* **2016**, *9*, 56–62.

52. Baranauskien, R.; Venskutonis, P. R.; Demyttenaere, J. C. R. Sensory and instrumental evaluation of sweet marjoram (Origanum majorana L .). aroma. *Flavour and fragrance journal*, **2005**, 492–500, https://doi.org/10.1002/ffj.1478.

53. Eddahhaoui, F. Z., Boudalia, M., Harhar, H., Chahboun, N., Tabyaoui, M., Guenbour, A., Zarrouk, A.; Bellaoucho, A. Effect of the extraction technique on the bioactive compounds and the antioxidant capacity of the Chamaerops humilis L. fruit (pulp and seeds), *Chemical Data Collections* **2022,** 100882, https://doi.org/10.1016/j.cdc.2022.100882.

54. Chien, S.Y; Sheen, S.; Sommers, C.; Sheen, L.Y. Combinatioe effect of high-pressure processing and essential oil (Melissa officinalis Extracts) or their constituents for the inactivation of *Escherichia coli* in ground beef. *Food and Bioprocess Technology*. **2019**, *12*, 359-70. https://doi.org/10.1007/s11947-018-2211-5.

55. Khadhri, A.; Masson, E.; Lagel, M. C.; Pizzi, A. Determination of phenolic compounds by MALDI – TOF and essential oil composition by GC – MS during three development stages of Origanum majorana L. *Biomedical Chromatography* **2019**, 1–13, https://doi.org/10.1002/bmc.4665.

56. Salha, B. Industrial Crops & Products Deterpenation of Origanum majorana L. essential oil by reduced pressure steam distillation. *Industrial Crops & Products* **2017** , *109*, 116–122, https://doi.org/10.1016/j.indcrop.2017.08.016.

57. Prior, R. L.; Wu, X.; Schaich, K. Standardized methods for the determination of antioxidant capacity and phenolics in foods and dietary supplements. *Journal of Agricultural and Food Chemistry* **2005,** *53*, 4290–4302, https://doi.org/10.1021/jf0502698.

58. Astani, A.; Reichling, J.; Schnitzler, P. Comparative Study on the Antiviral Activity of Selected Monoterpenes Derived from Essential Oils. *Phytotherapy Research* **2010** , *24*, 673–679, https://doi.org/10.1002/ptr.2955.

59. Oliveira, J. L. T. M.; de Fátima Melo Diniz, M.; de Oliveira Lima, E.; de Souza, E. L.; Trajano, V. N.; Santos, B. H. C. Effectiveness of Origanum vulgare L. and Origanum majorana L. essential oils in inhibiting the growth of bacterial strains isolated from the patients with conjunctivitis. *Brazilian Archives of Biology and Technology* **2009**, *52*, 45–50, https://doi.org/10.1590/S1516-89132009000100006.

60. Challouf, H.; Souissi, N.; Messaouda, M. Ben; Abidi, R.; Madani, A. Origanum majorana Extracts as Mild Steel Corrosion Green Inhibitors in Aqueous Chloride Medium. *Journal of Environmental Protection* **2016**, https://doi.org/10.4236/jep.2016.74048.

61. Al-Khaldi, M. A. Natural Products as Corrosion Inhibitor for Steel in 0.5 M Hydrochloric Acid Solution. *Asian Journal of Chemistry* **2016**, *28*, 2532–2538,

62. Beniken, M. Anticorrosion Activity of a Polyacrylamide with High Molecular Weight on C- Steel in Acidic Media : Part 1 Anticorrosion Activity of a Polyacrylamide with High Molecular Weight on C-Steel in Acidic Media : Part 1. *Journal of Bio- and Tribo-Corrosion* **2018**, https://doi.org/10.1007/s40735-018-0155-y.

63. Larouj, M.; Ourrak, K.; El M'Rabet, M.; Zarrok, H.; Serrar, H.; Boudalia, M.; Boukhriss, S.; Warad, I.; Oudda, H.; Touir, R. Thermodynamic study of corrosion inhibition of carbon steel in acidic solution by new pyrimidothiazine derivative. *Journal of Materials and Environmental Science* **2017**, *8*, 3921–3931.

64. Aourabi, S.; Driouch, M.; Kadiri, M.; Achnine, N.; Sfaira, M. Synergetic Effect between Phenolic Extracts of Ammi visnaga and Zea mays Formulation on the Corrosion of Mild Steel in 1 M HCl Solution. *Journal of Chemistry* **2021**, 2021.

65. Chami, R.; Boudalia, M.; Echihi, S., El Fal, M.; Bellaouchou, A.; Guenbour, A.;Tabyaoui, M.; Essassi, E.M.; Zarrouk, A.; Thermodynamic study and electrochemical Investigation of 4-chloro- 1H- pyrazolo [3 , 4-d] pyrimidine as a corrosion Inhibitor for mild steel in hydrochloric acid Solution, *Journal of Materials and Environmental Sciences*. **2017,** *8*, 4182–4192.

66. Afrokh, M.; Baroud, S.; Kerroum, Y.; Hatimi, A.; Tahrouch, S.; Sadki, I.; Warad, I.; Guenbour, A.; Bellaouchou, A.; Tabyaoui, M.; Zarrouk, A. Green Approach to Corrosion Inhibition of Carbon Steel by Fucus spiralis extract in 1 M HCl Medium. *Biointerface Research in Applied Chemistry* **2022**, *12*, 7075–7091, https://doi.org/10.33263/BRIAC125.70757091.

67. Z. Rouifi, M. El Faydy , H. About, F. Benhiba, H. Ramsis, M. Boudalia, H. Zarrok, R. Touir, M. El M'Rabet, H. Oudda, A. Guenbour, B. L. Electrochemical and theoretical studies of adsorption and corrosion inhibition of 1-methyl-4-methylsulfanyl- 1H-pyrazolo[3,4-d]pyrimidine on mild steel in acidic solution. *Journal of Materials and Environmental Science* **2018**, *9*, 453–465.

68. Mouflih, K.; Mouaden, K. El; Boudalia, M.; Bellaouchou, A.; Tabyaoui, M.; Guenbour, A.; Warad, I.; Zarrouk, A. The Effect of the Moroccan Salvadora Persica Extract on the Corrosion Behavior of the Ni–Cr Non-precious Dental Alloy in Artificial Saliva. *Journal of Bio- and Tribo-Corrosion* **2021**, *7*, 1–10, https://doi.org/10.1007/s40735-021-00495-7.

69. Ningshen, S.; Mudali, U. K.; Amarendra, G.; Raj, B. Corrosion assessment of nitric acid grade austenitic stainless steels. *Corrosion Science* **2009**, *51*, 322–329, https://doi.org/10.1016/j.corsci.2008.09.038.

70. Berrissoul, A.; Ouarhach, A.; Benhiba, F.; Romane, A.; Guenbour, A.; Outada, H.; Dafali, A.; Zarrouk, A. Exploitation of a new green inhibitor against mild steel corrosion in HCl: Experimental, DFT and MD simulation approach. *Journal of Molecular Liquids* **2022**, *349*, 118102, https://doi.org/10.1016/j.molliq.2021.118102.

71. Ningshen, S.; Mudali, U. K.; Mukherjee, P.; Sarkar, A.; Barat, P.; Padhy, N.; Raj, B. Influence of oxygen ion irradiation on the corrosion aspects of Ti-5 % Ta-2 % Nb alloy and oxide coated titanium. *Corrosion Science* **2008**, *50*, 2124–2134, https://doi.org/10.1016/j.corsci.2008.03.019.

72. Boudalia, M.; Guenbour, A.; Bellaouchou, A.; Laqhaili, A.; Mousaddak, M.; Hakiki, A., Hammouti, B. and Ebenso, E.E. A. Corrosion Inhibition of Organic Oil Extract of Leaves Of Lanvandula Stoekas on Stainless Steel in Concentrated Phosphoric Acid Solution. *International Journal of Electrochemical Science* **2013**, *8*, 7414.

73. Derfouf, H.; Harek, Y.; Larabi, L.; Basirun, W. J. Corrosion inhibition activity of carbon steel in 1.0 M hydrochloric acid medium using Hammada scoparia extract : gravimetric and electrochemical study hydrochloric acid medium using Hammada scoparia extract : gravimetric and electrochemical study. *Journal of Adhesion Science and Technology* **2019**, 1–26, https://doi.org/10.1080/01694243.2018.1562321.

74. Shukla, S. K.; Ebenso, E. E. Corrosion Inhibition , Adsorption Behavior and Thermodynamic Properties of Streptomycin on Mild Steel in Hydrochloric Acid Medium. *International Journal of Electrochemical Science* **2011**, *6*, 3277–3291.

75. Abdel-Gaber, A. M., Abd-El-Nabey, B. A., Sidahmed, I. M., El-Zayady, A. M., & Saadawy, M. Inhibitive action of some plant extracts on the corrosion of steel in acidic media. *Corrosion science* **2006**, *48*, 2765–2779, https://doi.org/10.1016/j.corsci.2005.09.017.

76. El Faydy, M.; Benhiba, F.; Warad, I.; About, H.; Saoiabi, S.; Guenbour, A.; Bentiss, F.; Lakhrissi, B.; Zarrouk, A. Experimental and theoretical investigations of two quinolin-8-ol derivatives as inhibitors for carbon steel in 1 M HCl solution. *Journal of Physics and Chemistry of Solids* **2022**, *165*, 110699, https://doi.org/10.1016/j.jpcs.2022.110699.

77. Ishwara Bhat, J., Alva Vijaya D.P. A Study of Aluminium Corrosion Inhibition in Acid Medium by an Antiemitic Drug. *Transactions of the Indian Institute of Metals* **2011**, *64*, 377–384, https://doi.org/10.1007/s12666-011-0102-9.

78. Laamari, M. R. Adsorption and corrosion inhibition of carbon steel in hydrochloric acid medium by hexamethylenediamine tetra (methylene phosphonic acid). *Arabian Journal of Chemistry* **2016**, *9*, 245–251, https://doi.org/10.1016/j.arabjc.2011.03.018.

79. El Faydy, M.; Benhiba, F.; Warad, I.; Abousalem, Ashraf S.; About, H.; Kerroum, Y.; Jama, C.; Guenbour, A.; Lakhrissi, B.; Zarrouk, A. Appraisal of corrosion inhibiting ability of new 5-N-((alkylamino)methyl) quinolin-8-ol analogs for C40E steel in sulfuric acid. *International Journal of Hydrogen Energy* **2021**, *46*, 30246–30266, https://doi.org/10.1016/j.ijhydene.2021.06.205.

80. Idouhli, R.; Oukhrib, A.; Khadiri, M.; Zakir, O.; Aityoub, A.; Abouelfida, A.; Benharref, A.; Benyaich, A. Understanding the corrosion inhibition effectiveness using Senecio anteuphorbium L. fraction for steel in acidic media. *Journal of Molecular Structure* **2021**, *1228*, 129478, https://doi.org/10.1016/J.MOLSTRUC.2020.129478.

81. Berrissoul, A.; Ouarhach, A.; Benhiba, F.; Romane, A.; Zarrouk, A.; Guenbour, A.; Dikici, B.; Dafali, A. Evaluation of Lavandula mairei extract as green inhibitor for mild steel corrosion in 1 M HCl solution . Experimental and theoretical approach. *Journal of Molecular Liquids* **2020**, *313*, 113493, https://doi.org/10.1016/j.molliq.2020.113493.

82. Leena, P., Zeinul Hukuman, N.H., Biju, A.R. and Jisha, M.. Studies on Methanolic Extract of Lepidagathis keralensis as Green Corrosion Inhibitor for Mild Steel in 1M HCl. *Journal of Electrochemical Science and Technology* **2019**, *10*, 231–243.

83. Goel, R.; Siddiqi, W. A.; Ahmed, B.; Shahid, M.; Chaubey, V. M. Synthesis characterization and corrosion inhibition ef fi ciency of N-C2 mild steel. *Desalination* **2010**, *263*, 45–57, https://doi.org/10.1016/j.desal.2010.06.033.

84. Gadow, H. S.; Motawea, M. M. (2017). Investigation of the corrosion inhibition of carbon steel in hydrochloric acid solution by using ginger roots extract. *RSC Advances* **2017**, *7*, 24576–24588, https://doi.org/10.1039/C6RA28636D.

85. Prabakaran, M.; Kim, S. H.; Kalaiselvi, K.; Hemapriya, V.; Chung, I. M. Highly efficient Ligularia fischeri green extract for the protection against corrosion of mild steel in acidic medium: Electrochemical and spectroscopic investigations. *Journal of the Taiwan Institute of Chemical Engineers* **2016**, *59*, 553–562, https://doi.org/10.1016/j.jtice.2015.08.023.

86. Şahin, E. A., Solmaz, R., Gecibesler, I. H., & Kardaş, G. Adsorption ability, stability and corrosion inhibition mechanism of phoenix dactylifera extrat on mild steel. *Materials Research Express* **2020**, *7*, 0–11, https://doi.org/10.1088/2053-1591/ab6ad3.

87. Bouoidina, A., El-Hajjaji, F., Emran, K., Belghiti, M.E., Elmelouky, A., Taleb, M., Abdellaoui, A., Hammouti, B. and Obot, I.B. Towards Understanding the Anticorrosive Mechanism of Novel Surfactant Based on Mentha pulegium Oil as Eco-friendly Bio-source of Mild Steel in Acid Medium : a Combined DFT and Molecular Dynamics Investigation. *Chemical Research in Chinese Universities* **2018**, *35*, 85-100, https://doi.org/10.1007/s40242-019-8205-7.

88. Obot, I. B., Haruna, K., Saleh, T. A. Atomistic Simulation : A Unique and Powerful Computational Tool for Corrosion Inhibition Research. *Arabian Journal for Science and Engineering* **2019**, https://doi.org/10.1007/s13369-018-3605-4.

89. Rouifi, Z.; Rbaa, M.; Benhiba, F.; Laabaissi, T.; Oudda, H.; Lakhrissi, B.; Guenbour, A.; Warad, I.; Zarrouk, A. Preparation and anticorrosion activity of novel 8-hydroxyquinoline derivative for carbon steel corrosion in HCl molar : Computational and experimental analyses. *Journal of Molecular Liquids* **2020**, *307*, 112923, https://doi.org/10.1016/j.molliq.2020.112923.

90. Olasunkanmi, L. O.; Obot, I. B.; Ebenso, E. E. Adsorption and corrosion inhibition properties of N-{n-[1-R-5-(quinoxalin-6- yl)-4,5-dihydropyrazol-3-yl]phenyl}methanesulfonamides on mild steel in 1 M HCl: Experimental and theoretical studies. *RSC advances* **2016**, *6*, 86782-86797.

91. Berrissoul, A.; Loukili, E.; Mechbal, N.; Benhiba, F.; Guenbour, A.; Dikici, B.; Zarrouk, A.; Dafali, A. Anticorrosion effect of a green sustainable inhibitor on mild steel in hydrochloric acid. *Journal of Colloid And Interface Science* **2020**, *580*, 740–752, https://doi.org/10.1016/j.jcis.2020.07.073.

92. Rahmani, H.; Alaoui, K. I.; EL Azzouzi, M.; Benhiba, F.; El Hallaoui, A.; Rais, Z.; Taleb, M.; Saady, A.; Labriti, B.; Aouniti, A.; Zarrouk, A. Corrosion assessement of mild steel in acid environment using novel triazole derivative as a anticorrosion agent: A combined experimental and quantum chemical study. *Chemical Data Collections* **2019**, *24*, 100302, https://doi.org/10.1016/j.cdc.2019.100302.

93. Elyaktini, A.; lachiri, A.; El F aydy, M.; F. Benhiba, H. Zarrok; azzouzi, M. EL; Zertoubi, M.; Azzi, M.; Lakhrissi, B.; Zarrouk, A. Practical and Theoretical Study on the Inhibitory Influences of New Azomethine Derivatives Containing an 8-Hydroxyquinoline Moiety for the Corrosion of Carbon Steel in 1 M HCl. *Oriental Journal of Chemistry* **2018,** *34*, 3016, https://doi.org/10.13005/ojc/340643.

94. Laabaissi, T.; Benhiba, F.; Rouifi, Z.; Rbaa, M.; Oudda, H.; Zarrok, Lakhrissi, B., Guenbour, A., Warad, I.; Zarrouk, A. Benzodiazepine Derivatives as Corrosion Inhibitors of Carbon Steel in HCl Media : Electrochemical and Theoretical Studies. *Protection of Metals and Physical Chemistry of Surfaces* **2019**, *55*, 986–1000, https://doi.org/10.1134/S2070205119050149.

95. Olasunkanmi, L. O., Obot, I. B., Kabanda, M. M., & Ebenso, E. E. Some Quinoxalin-6-yl derivatives as Corrosion Inhibitors for Mild Steel in Hydrochloric Acid : Experimental and Theoretical Studies. *The Journal of Physical Chemistry C* **2015**, *119*, 16004-16019.

96. Murmu, M.; Kr, S.; Chandra, N.; Banerjee, P. Effect of stereochemical conformation into the corrosion inhibitive behaviour of double azomethine based Schi ff bases on mild steel surface in 1 mol L − 1 HCl medium : An experimental , density functional theory and molecular dynamics simulation study. *Corrosion Science* **2019**, *146*, 134–151, https://doi.org/10.1016/j.corsci.2018.10.002.

97. About, H.; El Faydy, M.; Rouifi, Z.; Benhiba, F.; Ramsis, H.; Boudalia, M.; Zarrok, H.; Oudda, H.; Touir, R.; El M'Rabet, M.; Warad, I.; Guenbour, A.; Lakhrissi, B. Experimental and theoretical studies of 5-((4-phenyl-4,5-dihydro- 1H-tetrazol-1-yl)methyl)quinolin-8-ol quinoline derivative as effective corrosion inhibitor for mild steel in 1.0 M HCl. *Journal of Materials and Environmental Science* **2018**, *9*, 345–357, https://doi.org/10.26872/jmes.2018.9.1.38.

98. Saranya, J.; Benhiba, F.; Anusuya, N.; Subbiah, R.; Zarrouk, A.; Chitra, S. Experimental and computational

approaches on the pyran derivatives for acid corrosion. *Colloids and Surfaces A:Physicochemical and Engineering Aspects* **2020**, *603*, 125231, https://doi.org/10.1016/j.colsurfa.2020.125231.

99. Mehmeti, V.; Podvorica, F. I. Experimental and Theoretical Studies on Corrosion Inhibition of Niobium and Tantalum Surfaces by Carboxylated Graphene Oxide. *Materials* **2018**, *11*, 893, https://doi.org/10.3390/ma11060893.